Lithos 374–375 (2020) 105713

Contents lists available at ScienceDirect

Lithos

journal homepage: www.elsevier.com/locate/lithos

Research Article

Late Mesozoic magmatism at Xiaokelehe Cu—Mo deposit in Great Xing'an Range, NE China: Geodynamic and metallogenic implications

Yuzhou Feng [a,b], Huayong Chen [a,*], Bing Xiao [a], Rucao Li [a], Changzhou Deng [c], Jinsheng Han [a], Guanghui Li [c], Huilin Shi [c], Chunkit Lai [d]

[a] Guangzhou Institute of Geochemistry, Chinese Academy of Science, Guangzhou 510640, China
[b] University of Chinese Academy of Science, Beijing 100049, China
[c] Heilongjiang Institute of Geological Survey, Harbin 150036, China
[d] Faculty of Science, Universiti Brunei Darussalam, Gadong BE1410, Brunei Darussalam

ARTICLE INFO

Article history:
Received 17 April 2020
Received in revised form 22 July 2020
Accepted 23 July 2020
Available online 28 July 2020

Keywords:
Late Mesozoic magmatism
Mongol-Okhotsk Ocean
Mantle source
Porphyry Cu—Mo deposit
Great Xing'an Range

ABSTRACT

Multiphase Late Mesozoic magmatism is clearly recorded at the Xiaokelehe porphyry Cu—Mo deposit in NE China, including the *syn*-ore granodiorite porphyry, and post-ore diorite, gabbro, monzonite (porphyry), and granite porphyry. In this study, we present new geological, LA-ICP-MS zircon U—Pb geochronological and geochemical data on these intrusive units to unravel the tectonic evolution of the Late Mesozoic Great Xing'an Range (GXR). Zircon U—Pb dating indicates that the multiphase magmatism extended from the Late Jurassic to Early Cretaceous, i.e., 149.4 ± 4.0 Ma (diorite), 148.9 ± 1.4 Ma (granodiorite porphyry), 146.9 ± 4.1 Ma (monzonite), 140.6 ± 3.8 Ma (gabbro), and 139.9 ± 4.3 Ma (monzonite porphyry).

Geochemical data indicate that the *syn*-ore granodiorite porphyry is adakie-like, featured by relatively LILE-enrichments (Rb, Ba, K, Pb, LREEs), high Sr contents (1065–1130 ppm), and elevated Sr/Y (129.9–171.8) and $(La/Yb)_N$ (35.12–47.07) ratios, but with HFSE-depletions (Nb, Ta, Ti, HREEs), low Y (6.2–8.7 ppm) and Yb (0.48–0.67) contents. The granodiorite porphyry has relatively higher $Mg^{\#}$ values (41–47), depletion of Nb and Ta, low Cr (29.0–31.0 ppm) and Ni contents (9.4–12.6 ppm), as well as enriched Sr—Nd isotope features, indicating that the granodiorite porphyry was derived from an enriched mantle (garnet-bearing) refertilized by subduction-related melts in a post-collision setting, and the magmas were subsequently fractionated during their ascent. The diorite and gabbro may have also derived from the refertilized lithospheric mantle (but without garnet), whereas the monzonite and its porphyry were derived from the lower crust at >40 and < 40 km depths, respectively. Meanwhile, fractionation and crustal assimilation have been important for the diorite, gabbro, and monzonite (porphyry) formation. Combined our study with published ones, we concluded that: (1) the Mongol-Okhotsk Ocean was finally closed in the GXR before the Late Jurassic; and (2) Late Mesozoic magmatism and porphyry Cu—Mo mineralization in the GXR likely occurred in the compressive-to-extensional transition after the collision between the Mongol-SinoKorea and Siberia plates.

1. Introduction

The Great Xing'an Range (GXR) is located in the eastern Central Asian Orogenic Belt (CAOB), and contains voluminous Mesozoic magmatic rocks and their associated porphyry-type deposits (Chen et al., 2017). The GXR therefore provides a window to investigate the petrogenesis, geodynamic setting, and mineralization of the eastern CAOB. Despite many previous studies on the geology, geochronology, geochemistry and mineralization relations of these Mesozoic rocks in the GXR (Dai et al., 2020; Deng et al., 2019a, 2019b; Shu et al., 2016; Tang et al., 2016; Wang et al., 2006, 2015; Xu et al., 2013; Yang et al., 2015), considerable debate still remains on the Late Mesozoic petrogenetic setting, including partial melting of the (1) subducted Paleo-Pacific slab (Shu et al., 2016); (2) subducted Mongol-Okhotsk oceanic plate (Deng et al., 2019a, 2019b; Donskaya et al., 2013); (3) lower crust or an enriched mantle in a post-collision setting (Liu et al., 2013; Sorokin et al., 2020; Tang et al., 2016; Xu et al., 2013; Yang et al., 2015), and (4) ancient hydrous slab of the already-closed Paleo-Asian Ocean (i.e., deep-sourced water-fluxed melting model) (Li et al., 2017a, 2017b). The debate was partly caused by different sample locations and limited Late Mesozoic igneous outcrops in the GXR.

The GXR contains many porphyry-type deposits, and are mostly Mo-only or Mo-dominated. The few Cu-dominated ones include the Duobaoshan, Tongshan (506 ± 14 Ma; Chen et al., 2017; Cai et al., 2020), Wunugetushan (180.5 ± 2.0 Ma; Wang et al., 2015), Fukeshan

* Corresponding author.
E-mail address: huayongchen@gig.ac.cn (H. Chen).

https://doi.org/10.1016/j.lithos.2020.105713
0024-4937/

(148.7 ± 0.8 Ma; Deng et al., 2019a), and Xiaokelehe (150 Ma; Feng et al., 2019). Occurrence of the Wunugetushan, Fukeshan and Xiaokelehe deposits suggests substantial Late Mesozoic porphyry Cu(—Mo) mineralization potential in the GXR. The Xiaokelehe deposit is a newly-discovered large Cu—Mo deposit (Feng et al., 2019). A total of 42 holes have been drilled (total core length: 45000 m), which intersect various types of Late Mesozoic magmatic rocks that are not encountered on surface outcrops, and makes Xiaokelehe an ideal site to study the geology and tectonic setting of the Late Mesozoic GXR. Deng et al. (2019b) has obtained zircon U—Pb ages for the rhyolite (152.5 ± 1.7 Ma), granodiorite porphyry (150.0 ± 1.6 Ma), diorite porphyry (147.9 ± 1.3 Ma) and granite porphyry (123.2 ± 1.7 Ma) at Xiaokelehe, yet Shang (2017) reported a different zircon U—Pb age for the granodiorite porphyry ore host (~142 Ma). This shows a prolonged or multiphase magmatism that extended from the Late Jurassic to the Early Cretaceous. Based on geochemical evidence, granodiorite porphyry was interpreted to be related to the Mongol-Okhotsk Ocean subduction (Deng et al., 2019b). However, an earlier rhyolite suite was identified as A-type (Deng et al., 2019b), suggesting an extensional setting instead of a compressive continental arc setting (Xu et al., 2013). Besides, the various types of dykes (e.g., diorite, monzonite (porphyry), gabbro) intersected in the drill holes at Xiaokelehe have not been studied in detail, which limits our understanding of the magmatic-metallogenic evolution at Xiaokelehe, and in the GXR as a whole.

Therefore, we conducted systematic analyses on the geology, age and geochemical features of the granodiorite porphyry, diorite, monzonite (porphyry), and gabbro at Xiaokelehe. Our results elucidate the petrogenesis of these intrusive bodies, and their implications on the tectono-metallogenic evolution of the Late Mesozoic GXR.

2. Geological setting

The GXR is situated in the eastern CAOB that lies between the Siberian plate in the north and the SinoKorean-Tarim plate in the south (Fig. 1a). The GXR was evolved from the closure of the Paleo-Asian and Mongol-Okhotsk Oceans, as well as the subduction of the Paleo-Pacific oceanic plate, accompanied by multiple terrane accretion and continental crust growth that lasted from the Paleozoic to Cenozoic (e.g., Chen et al., 2017; Dai et al., 2020). This current GXR consists of a tectonic collage of micro-continental blocks/slivers, arc terranes and ophiolite belts of varying ages. Major tectonic terranes in the GXR (from north to south) include the Erguna, Hingan and Xilinhot, which are bordered by the Derbugan and Hegenshan-Heihe faults, respectively (Fig. 1b; e.g., Chen et al., 2017). The NNE-trending Derbugan Fault (900 km long, 10–30 km wide) extends from Mongolia, through the GXR to the Russia Far East. Regional stratigraphy in the GXR comprises Precambrian to Paleozoic, Jurassic-Cretaceous and Cenozoic sequences. Precambrian metamorphic basement (meta-volcanic-sedimentary) rocks were reported mainly in the eastern Erguna terrane (and sporadically in the NW Hingan terrane) (Chen et al., 2017; Shang, 2017). The Lower Paleozoic rocks are only exposed in the Hingan terrane, and are composed of terrigenous (volcani) clastic rocks and marine carbonates (Shang, 2017). The Upper Paleozoic rocks outcrop mainly in the Hingan terrane, and are dominated by low-grade metamorphosed volcanic-sedimentary rocks (Shang, 2017). Jurassic-Cretaceous terrigenous (volcanic) clastic rocks are widespread across the whole GXR (Deng et al., 2018a, 2018b; Deng and Li, 2019), whilst Cenozoic terrigenous clastic sediments are mainly exposed in the eastern Hingan terrane (Chen et al., 2017). Regional tectonomagmatic events in the GXR fall into four episodes: (1) Paleozoic continental arc magmatism associated with the subduction of Paleo-Asia Ocean (Li et al., 2013a; Liu et al., 2020; Xu et al., 2013); (2) Early-Middle Triassic and (3) Late Triassic and Early Jurassic continental arc magmatism related to the subduction of Mongol-Okhotsk Ocean (mainly in the northern GXR) (Li et al., 2013a; Xu et al., 2013) and/or post-collisional extension after the Paleo-Asia Ocean closure (mainly in the southern GXR) (Li et al., 2013a); (4) Middle-Late Jurassic and Cretaceous continental-arc magmatism associated with subduction of the Mongol-Okhotsk Ocean (Deng et al., 2019a, 2019b), or post-collision magmatism after the closure

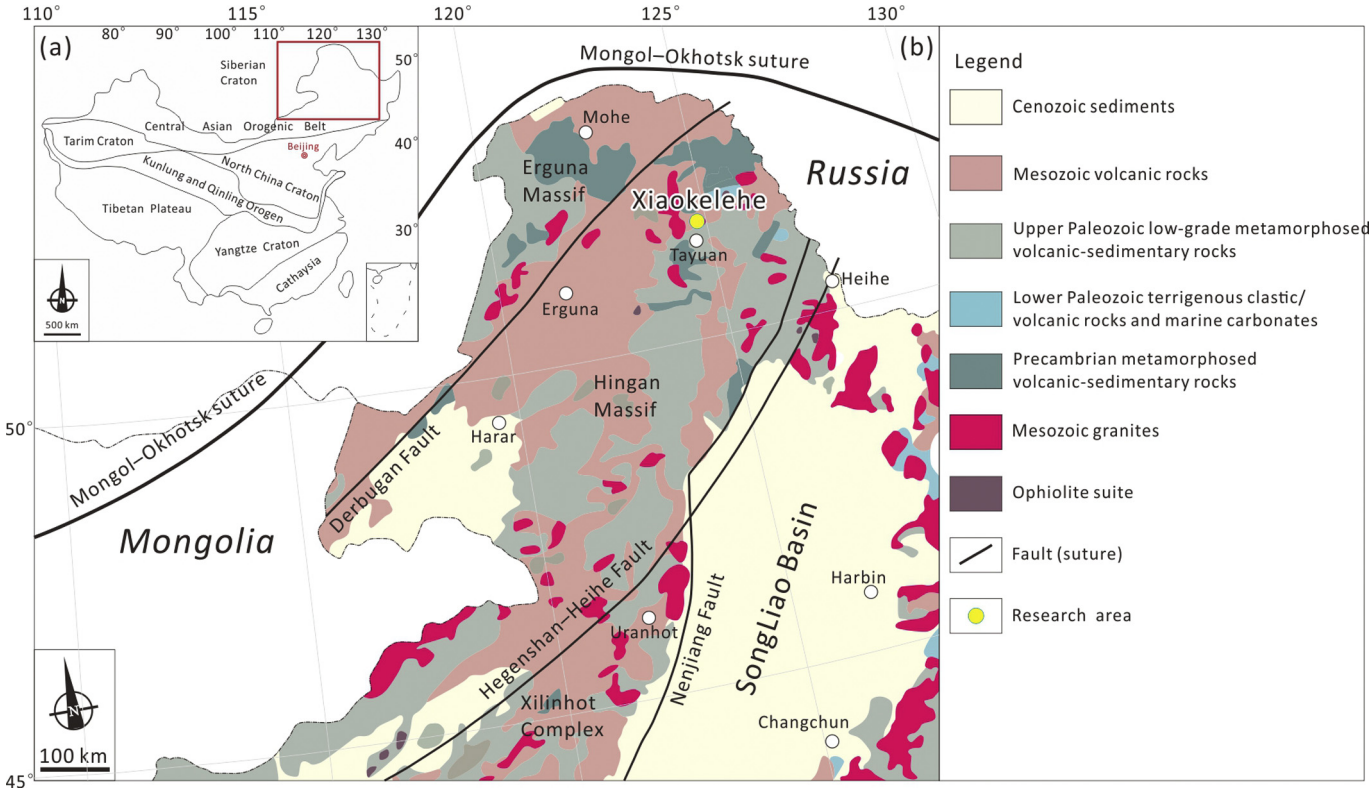

Fig. 1. (a) Simplified map showing the location of the Great Xing'an Range in the eastern Central Asian Orogenic Belt; (b) Geologic map of the Great Xing'an Range, showing the location of Xiaokelehe Cu—Mo deposit (modified after Chen et al., 2017).

of the Mongol-Okhotsk Ocean (Sorokin et al., 2020; Zhang, 2014) or the Paleo-Asia Ocean (Li et al., 2017a, 2017b). Such multistage Mesozoic tectono-magmatic activities also induced widespread porphyry-type mineralization (mostly Mo with minor Cu—Mo) (Chen et al., 2017).

The Xiaokelehe Cu—Mo deposit lies in the eastern Hingan terrane, about 25 km northeast of the Tayuan city (Fig. 2a). Local stratigraphy comprises Neoproterozoic and Late Jurassic volcanic-sedimentary units (Shang, 2017). The Neoproterozoic rocks are widely exposed at Xiaokelehe, and comprise mainly meta-sandstones, slate, phyllite, schist and marble. The Late Jurassic rocks are exposed in the southern and western Xiaokelehe, and are dominated by dacitic-rhyolitic lava and tuff (Shang, 2017). These Neoproterozoic and Upper Jurassic wallrocks around the granodiorite porphyry are mildly Cu—Mo mineralized. The NE-trending Xiaokelehe and NW-trending Dawusu faults dissected the Neoproterozoic rocks and controlled the distribution of the Mesozoic magmatism and associated mineralization (Shang, 2017). The highly-fractured granodiorite porphyry may have also facilitated the quartz-sulfides stockwork mineralization. Late Mesozoic igneous rocks are extensively developed at Xiaokelehe, and include Late Jurassic volcaniclastic rocks, granodiorite porphyry, diorite (porphyry), monzonite (porphyry) and gabbro, together with Early Cretaceous granite porphyry (Fig. 2b). These rock types are similar to those reported outside Xiaokelehe in the Mesozoic GXR.

3. Petrography

Based on our field observations, we have divided the magmatic rocks at Xiaokelehe into *syn*-ore and post-ore ones, and their contact relationships and petrographic characteristics are presented in Figs. 3 and 4.

3.1. Syn-ore magmatic rocks

The syn-ore granodiorite porphyry outcrop covers about 4.5 km^2 at Xiaokelehe (Fig. 2a), and intruded into the Neoproterozoic metamorphosed clastic rocks and the Late Jurassic volcanic rocks (Fig. 2b). These rocks are grayish-white (Fig. 4a), and have phenocrysts of quartz (25–30 vol%), plagioclase (~40 vol%), biotite (10–15 vol%), and minor hornblende (<5 vol%) and K-feldspar (<10 vol%), with grain sizes of 2.0–8.0 mm. The groundmass is composed of quartz, plagioclase and K-feldspar. Accessory minerals (<5 vol%) include magnetite, apatite and zircon (Figs. 4b-c). As the main ore host, the granodiorite porphyry is pervasively altered and mineralized, with the sodic-calcic, potassic, chlorite-illite and phyllic alterations centered on the granodiorite porphyry, and the Cu—Mo mineralization occurs mainly in the potassic zone, as described in detail by Feng et al. (2019).

3.2. Post-ore magmatic rocks

Diorite occurs as dykes and intruded into the granodiorite porphyry (along sharp intrusive contact), the Neoproterozoic metamorphosed clastic rocks and the Late Jurassic volcanic rocks, with width of ca. 1–10 m (Fig. 2a). Diorite dykes crosscut also the quartz-sulfide ore veins in the granodiorite porphyry, suggesting that they are post-ore (Fig. 3a). These rocks are greenish-gray, weakly chlorite-altered and medium-fine grained (<1–4 mm) (Fig. 4d). The diorite is made up of plagioclase (70 vol%), K-feldspar (10 vol%), pyroxene (10 vol%), hornblende (5 vol%) and quartz (5 vol%). Accessory minerals (<5 vol%) include magnetite, apatite and zircon (Fig. 4e-f).

Monzonite occurs as dykes or stocks with widths of 1 to 110 m and intruded the granodiorite porphyry along sharp baked/chilled contact (Fig. 2b). Meanwhile, intense potassic alteration occurs in the granodiorite porphyry along the granodiorite-monzonite contact (Fig. 3b), which is likely caused by the monzonite intrusion. These rocks are greenish-gray, weakly-altered and fine-grained (0.05–0.3 mm) (Fig. 4g). The monzonite contains mainly plagioclase (45 vol%), K-feldspar (40 vol %), pyroxene (5 vol%), hornblende (<5 vol%) and quartz (<5 vol%). Accessory minerals (<5 vol%) include magnetite, apatite and zircon (Fig. 4h-i).

Gabbro is found only locally at Xiaokelehe, and occurs as dykes intruding all the Neoproterozoic and Late Jurassic wallrocks, granodiorite porphyry, diorite, and monzonite along sharp contacts (Figs. 2b, 3c-d). Local breccias of Neoproterozoic wallrocks are concentrated around the gabbroic dykes. The gabbro is greenish-gray, weakly chlorite-altered, fine-grained (0.1–3 mm), and mainly contains plagioclase (60 vol%), pyroxene (25 vol%) and K-feldspar (10 vol%) (Fig. 4j-l). Accessory minerals (<5 vol%) include magnetite, apatite and zircon. The subhedral pyroxene grains are included in euhedral plagioclase.

Monzonite porphyry occurs as dykes (1–10 m wide) intruding the Neoproterozoic and Late Jurassic wallrocks, granodiorite porphyry, diorite, and monzonite along sharp baked/chilled contact (Figs. 2b

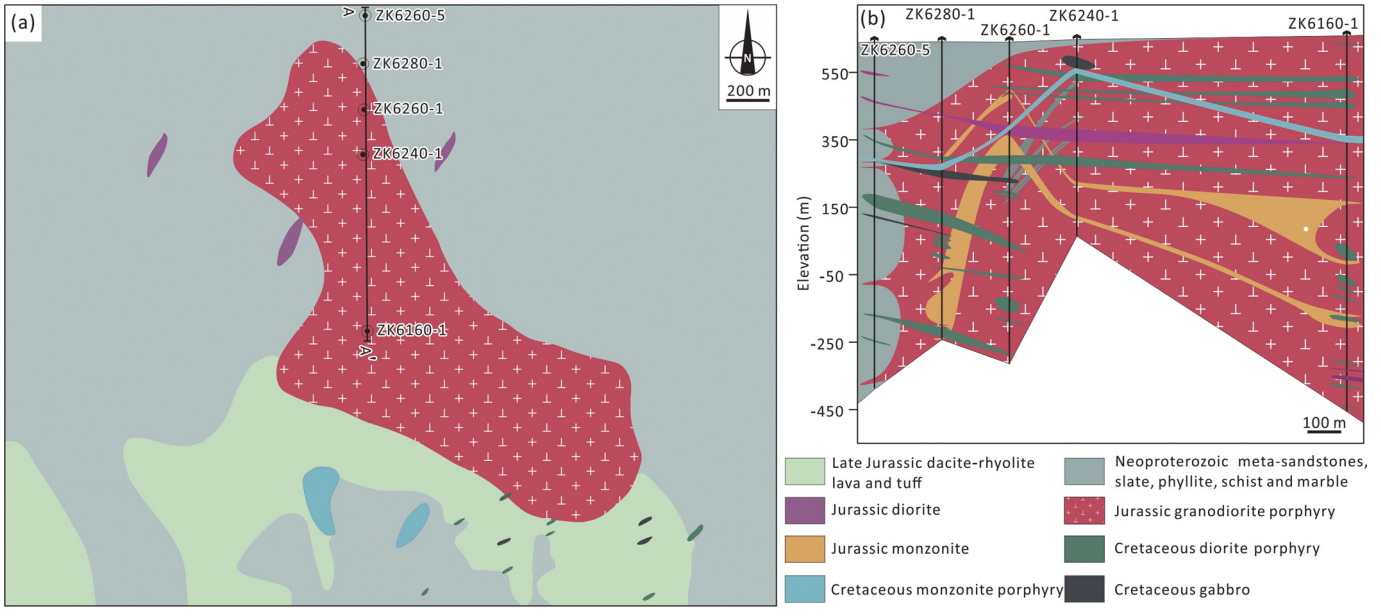

Fig. 2. (a) Geologic map of the Xiaokelehe ore district, showing locations of drill holes and the CC' profile, (b) Geological cross-section CC' (modified after Feng et al., 2019).

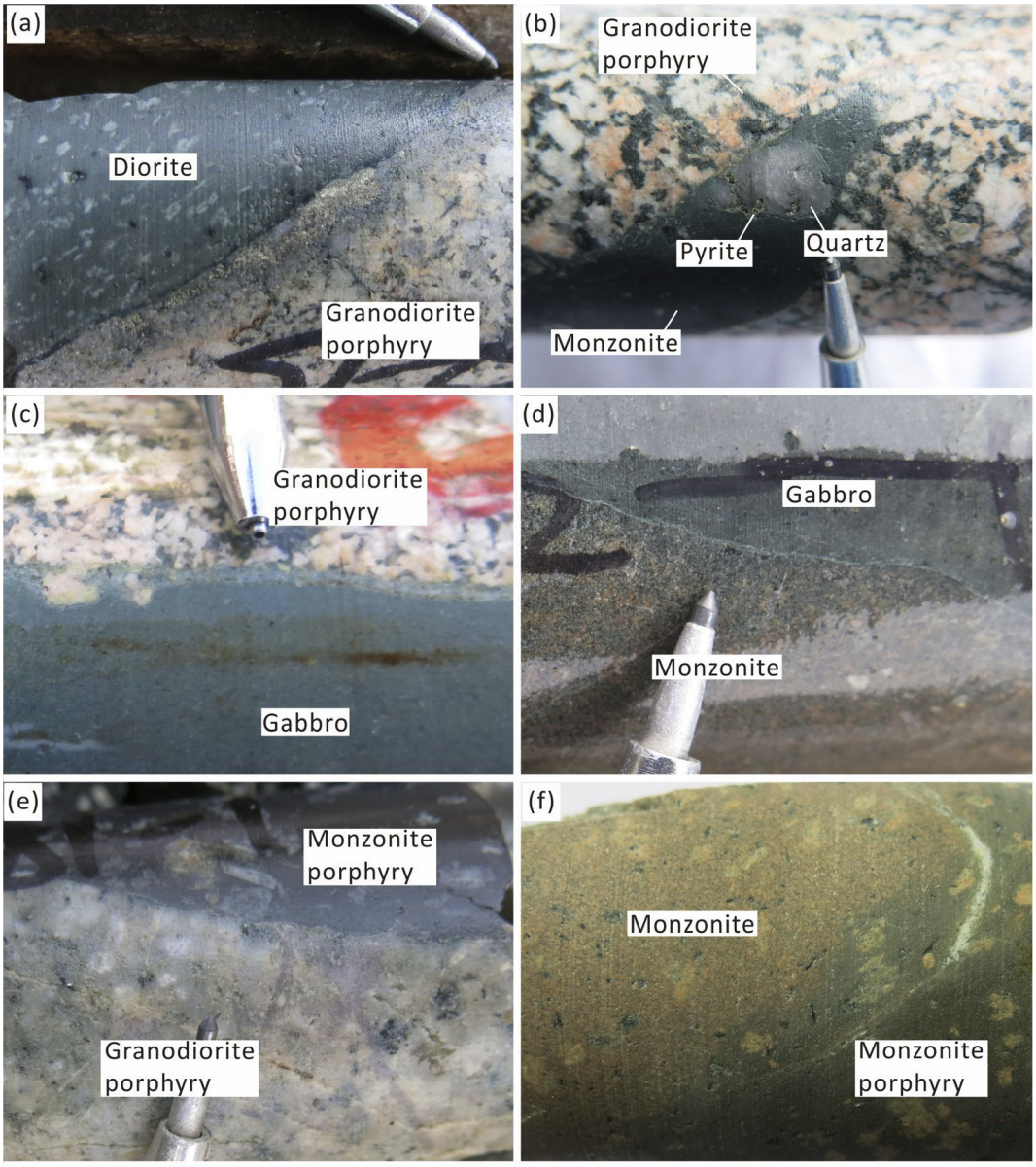

Fig. 3. Photographs showing the crosscutting relations between the major magmatic units at Xiaokelehe. (a) Rhyolite (in contact with granodiorite porphyry) is intensely phyllic altered; (b) Sharp intrusive contact between granodiorite porphyry and diorite. Sulfides-bearing veins in the granodiorite porphyry also cut by the diorite; (c) Diorite porphyry intruded granodiorite porphyry with sharp chilled/baked margin; (d) Sharp intrusive contact between granodiorite porphyry and monzonite, with quartz-sulfides breccias in the monzonite close to the contact; (e) Gabbro intruded granodiorite porphyry along sharp contact, with the latter being intensely K-feldspar altered locally; (f) Gabbro intruded monzonite along sharp contact; (g) Monzonite porphyry intruded granodiorite porphyry along sharp contact. Quartz veins in the granodiorite porphyry cut by the monzonite porphyry; (h) Monzonite intruded by monzonite porphyry along sharp contact with intense K-feldspar alteration; (i) Granite porphyry intruded granodiorite porphyry along sharp contact.

and 3e-f). Quartz-sulfides veins were cut by monzonite porphyry dykes (Fig. 3g), indicating a post-ore origin for the latter. These rocks are grayish in color and weakly-altered (Fig. 4m). The phenocrysts comprise plagioclase (20 vol%) and pyroxene (10 vol%), with grain sizes from 0.5 to 5 mm. The groundmass is microcrystalline and consists of mostly feldspar and minor quartz. Accessory minerals (<5 vol%) include magnetite, apatite and zircon (Fig. 4n-o).

4. Sampling and methods

As mentioned above, controversies exist on the formation ages of the granodiorite porphyry, and no ages were reported on the newly-identified diorite, monzonite (porphyry) and gabbro. Therefore, in this study, we conducted LA-ICP-MS zircon U—Pb dating and major/trace element compositions of the least-altered granodiorite porphyry, diorite, monzonite (porphyry) and gabbro samples at Xiaokelehe. The sampling locations and lithologies of the magmatic rocks analyzed are presented in Table 1.

One sample each from the Xiaokelehe granodiorite porphyry (ZK6280-1-3), diorite (ZK6280-1-2), monzonite (ZK6280-1-1), gabbro (ZK6260-5-1) and monzonite porphyry (ZK6240-1-1) were chosen for zircon U—Pb dating. Zircon grains were separated from samples using conventional heavy liquids and magnetic separation techniques, and handpicked under a binocular microscope. Zircon CL images were obtained using a TESCAN MIRA3 field-emission scanning electron microprobe (FE-SEM) at the Testing Center, Tuoyan Analytical Technology Co. Ltd. (Guangzhou, China). Working conditions of the CL imaging were described in detail by Zhang et al. (2019). The LA-ICP-MS zircon U—Pb dating and trace element analyses were determined at the Key Laboratory of Marine Resources and Coastal Engineering, Sun Yat-sen

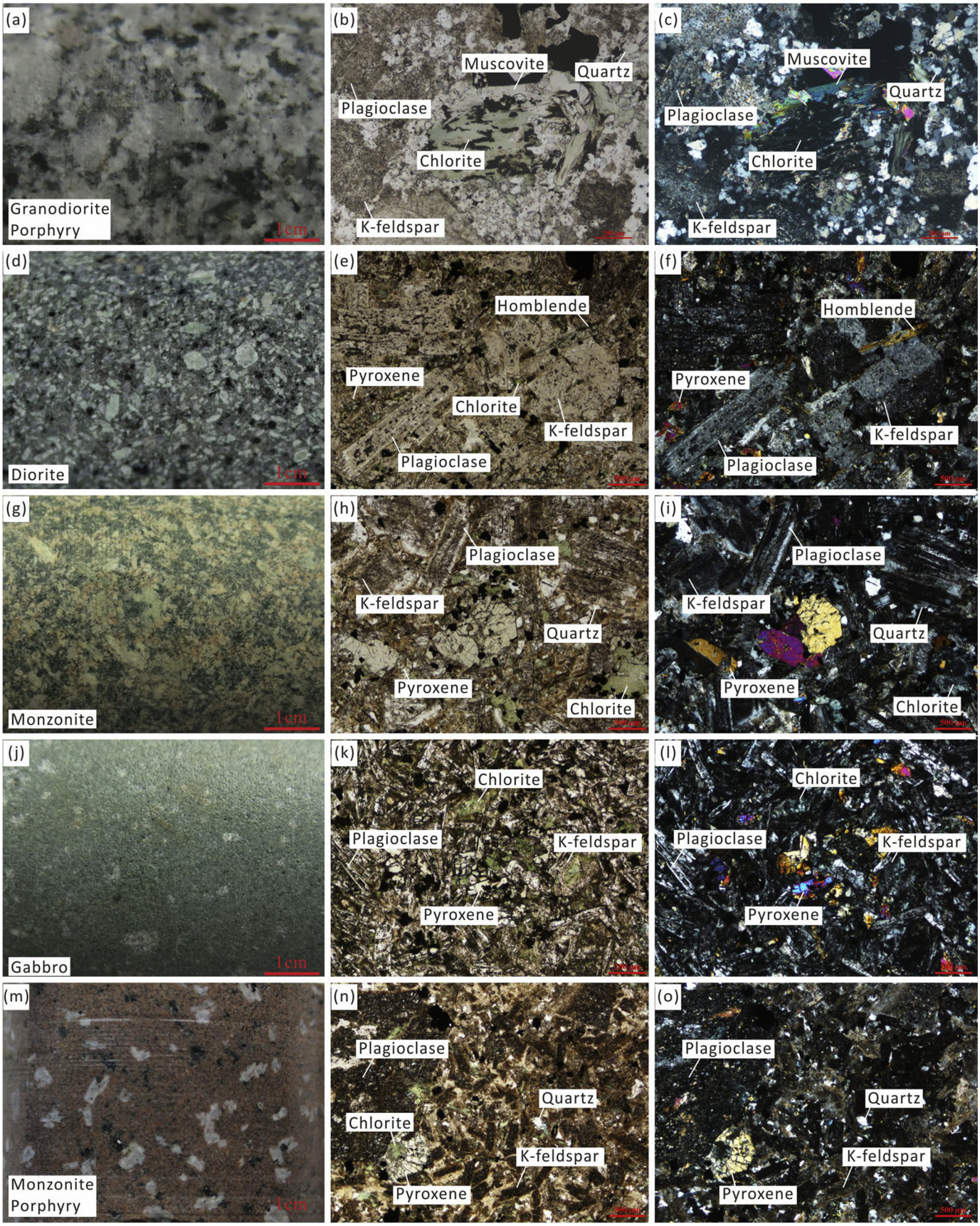

Fig. 4. Hand-specimen photos and thin-section microphotographs of the major magmatic units at Xiaokelehe. (a-c) Chlorite-illite- and phyllic-altered granodiorite porphyry. Chlorite altered from biotite and replaced by muscovite, plagioclase and K-feldspar altered to clay minerals; (d-f) Weakly-altered diorite containing hornblende, pyroxene, plagioclase and K-feldspar; (g-i) Weakly-altered monzonite containing mainly pyroxene, plagioclase and K-feldspar, and minor quartz; (j-l) Weakly-altered gabbro containing mainly pyroxene, plagioclase and K-feldspar; (m-o) Weakly-altered monzonite porphyry containing mainly pyroxene, plagioclase and K-feldspar, and minor quartz.

Table 1
Sample location and features of the main magmatic rocks at Xiaokelehe.

Sample no.	Drilling	Lithology	Location		
			Easting	Northing	Depth
ZK6280-1-80	ZK6280-1	Granodiorite porphyry	21606143.8	5729303.9	83.6
ZK6280-1-84	ZK6280-1	Granodiorite porphyry	21606143.8	5729303.9	54.6
ZK6280-1-77	ZK6280-1	Diorite	21606143.8	5729303.9	103.6
ZK6280-1-99	ZK6280-1	Diorite	21606143.8	5729303.9	−48.4
ZK6280-1-117	ZK6280-1	Monzonite	21606143.8	5729303.9	−175.4
ZK6280–1-120	ZK6280-1	Monzonite	21606143.8	5729303.9	−195.4
ZK6280-1-121	ZK6280-1	Monzonite	21606143.8	5729303.9	−204.4
ZK6260-5-122	ZK6260-5	Gabbro	21606153.8	5729101.4	−242.3
ZK6260-5-123	ZK6260-5	Gabbro	21606153.8	5729101.4	−251.3
ZK6260-5-133	ZK6260-5	Gabbro	21606153.8	5729101.4	−321.3
ZK6280-1-53	ZK6280-1	Monzonite porphyry	21606143.8	5729303.9	272.6
ZK6240-1-14	ZK6240-1	Monzonite porphyry	21606145.2	5728902.9	553.6
ZK6160-1-88	ZK6160-1	Monzonite porphyry	21606149.8	5728095.5	28.6
ZK6160-1-94	ZK6160-1	Monzonite porphyry	21606149.8	5728095.5	−7.4

University. The analyses were conducted using 193 nm ArF excimer laser ablation system (GeoLasPro) coupled with an Agilent 7700x ICP-MS. A 60 μm spot size was used with an energy density of 5 J/cm^2 and a repetition rate of 5 Hz. Zircon 91,500 and glass NIST610 were used as external standards for U—Pb dating and trace element calibration, respectively (Li et al., 2019). An Excel-based software ICPMSDataCal was used to perform off-line selection and integration of background and analyzed signals, time-drift correction and quantitative calibration for trace element analysis and U—Pb dating (Liu et al., 2010). Concordia diagrams and weighted mean calculations were created using Isoplot/Ex_ver3 (Ludwig, 2003).

Major and trace elements analyses were conducted at the ALS Mineral/ALS Chemex Co. Ltd. (Guangzhou, China). Major oxide contents were determined by XRF spectrometry. Fused glass disks with Lithium Borate were used and the analytical precisions were better than ±0.1%, based on repeated analyses of the standards GSR-2 and GSR-3. Trace element concentrations were determined by ICP-MS. Analyses of USGS rocks standards (BCR-2, BHVO-1 and AGV-1) reveal that the precision and accuracy were better than ±5% for the trace elements studied. Detailed analytical method and procedure were given in Zhang et al. (2019).

5. Results

5.1. Zircon U—Pb age

The results of zircon U—Pb dating of five samples are listed in Supplementary Appendix 1. Representative CL images of the analyzed zircons and zircon U—Pb concordia diagrams are illustrated in Supplementary Appendix 2 and Fig. 5. Regardless of the rock types, all the zircons analyzed are euhedral-subhedral, and show fine-scale oscillatory igneous growth zoning in CL images.

5.1.1. Granodiorite porphyry

The oscillatory zoning and elevated Th/U ratios (0.60–1.20) suggest an igneous origin for the zircons (Hoskin and Schaltegger, 2003). The $^{206}Pb/^{238}U$ ages of 18 analysis spots range from 144.2 ± 2.3 Ma to 153.9 ± 3.2 Ma, yielding a weighted mean $^{206}Pb/^{238}U$ age of 148.9 ± 1.4 Ma (MSWD = 0.59, n = 18) (Fig. 5a).

5.1.2. Diorite

The oscillatory zoning and elevated Th/U ratios (0.61–1.32) of the zircons reflect an igneous origin. The $^{206}Pb/^{238}U$ ages of 8 analysis spots range from 143.4 ± 2.8 Ma to 155.1 ± 2.4 Ma, yielding a weighted mean $^{206}Pb/^{238}U$ age of 149.4 ± 4.0 Ma (MSWD = 2.1, n = 6) (Fig. 5b). Two inherited zircons of 176.2 ± 5.4 Ma and 315.9 ± 6.9 Ma are also identified.

5.1.3. Monzonite

The oscillatory zoning and elevated Th/U ratios (0.46–2.46) reflect an igneous origin for the zircons. The $^{206}Pb/^{238}U$ ages of 11 analysis spots are from 143.7 ± 3.8 Ma to 323.1 ± 6.8 Ma, yielding three groups of weighted mean ages of 146.9 ± 4.1 Ma (MSWD = 1.06, n = 2), 191.8 ± 3.4 Ma (MSWD = 0.62, n = 6) and 309 ± 22 Ma (MSWD = 3.8, n = 3) (Fig. 5c). The youngest age (146.9 Ma) is recognized to represent the crystallization age of the monzonite.

5.1.4. Gabbro

The oscillatory zoning and elevated Th/U ratios (0.26–2.87) of the zircons reflect an igneous origin. The $^{206}Pb/^{238}U$ ages of six analysis spots are from 137.5 ± 3.6 Ma to 237.6 ± 4.1 Ma, yielding two groups with weighted mean ages of 140.6 ± 3.8 Ma (MSWD = 0.77, n = 3) and 234.3 ± 4.5 Ma (MSWD = 0.98, n = 3) (Fig. 5d). The younger age is considered to represent the monzonite formation age. Moreover, four inherited zircons (1860.5 ± 20.7 Ma, 1980.1 ± 19.3 Ma, 2337.2 ± 22.7 Ma and 2433.8 ± 42.7 Ma) are identified.

5.1.5. Monzonite porphyry

The oscillatory zoning and elevated Th/U ratios (0.26–1.81) of the zircons reflect an igneous origin. The $^{206}Pb/^{238}U$ ages of two analysis spots are of 136.1 ± 3.8 Ma and 141.8 ± 2.6 Ma, yielding a weighted mean age of 139.9 ± 4.3 Ma (MSWD = 1.5, n = 2) (Fig. 5e). Besides, three inherited zircons (176.1 ± 3.6 Ma, 295.1 ± 7.6 Ma and 2425 ± 23.6 Ma) are identified.

5.2. Major and trace element compositions

Whole-rock geochemical data of two granodiorite porphyry, two diorite, two monzonite, three gabbro and four monzonite porphyry samples are listed in Supplementary Appendix 3. The results show that all samples have low LOI (0.74–3.28), and are plotted within "the least altered field" in the alteration box (Fig. 6a; Large et al., 2001). Thus, geochemical influenced by hydrothermal alteration in the studied samples is likely insignificant (Asadi et al., 2014).

5.2.1. Granodiorite porphyry

The samples have SiO_2 = 63.68–67.55 wt% (avg. 65.62 wt%), Total Fe_2O_3 = 3.63–4.46 wt% (avg. 4.05 wt%), and $Mg^{\#}$ = 41–47 (avg. 44). In the TAS diagram (Fig. 6b; Irvine and Baragar, 1971) and K_2O vs. SiO_2 diagram (Fig. 6c; Peccerillo and Taylor, 1976), the granodiorite porphyries are plotted in the subalkaline and high-K calc-alkaline fields. Their A/CNK values (0.90–1.00) suggest a metaluminous nature (Fig. 6d; Maniar and Piccoli, 1989). The TFe_2O_3, MgO, Al_2O_3, TiO_2, CaO and P_2O_5 contents are negatively correlated with the SiO_2 contents, whereas K_2O contents show an opposite trend (Fig. 7). Meanwhile, the granodiorite porphyry samples are enriched in LREEs [$(La/Yb)_N$ = 35.12–47.07], LILEs (Rb, Ba, K and Pb) and Sr contents (1065–1130 ppm), and depleted in HREEs, HFSEs (Nb, Ta and Ti), Cr (29.0–31.0 ppm), Ni (9.4–12.6 ppm) and Y contents (6.2–8.7 ppm) (Fig. 8a-b). The rocks are featured by high Sr/Y ratios (63.6–73.6) and no Eu anomaly (δEu = 0.95–1.02), suggesting an adakitic affinity (Fig. 8c-d).

5.2.2. Diorite

The samples have SiO_2 = 54.83–56.04 wt% (avg. 55.44 wt%), Total Fe_2O_3 = 7.24–7.73 wt% (avg. 7.49 wt%), and $Mg^{\#}$ = 50–52 (avg. 51). The rocks are (high-K) calc-alkaline (Figs. 6b-c). Their A/CNK values vary from 0.87 to 0.93, indicating that the diorite is metaluminous (Fig. 6d). Correlation are subtle between the TFe_2O_3, MgO, Al_2O_3, TiO_2,

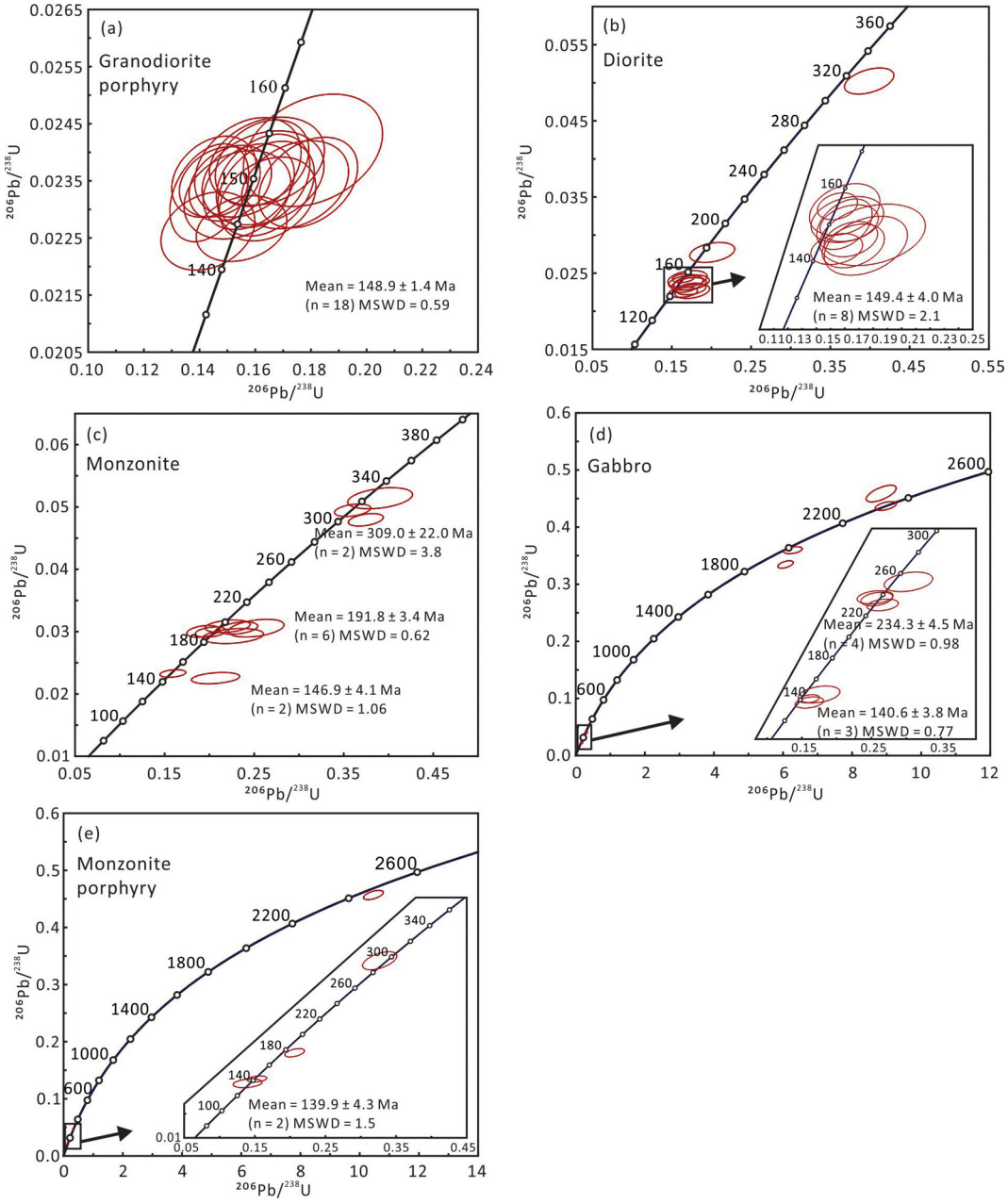

Fig. 5. Zircon U—Pb Concordia diagrams and relative probability plot for the granodiorite porphyry (a), diorite (b), monzonite (c), gabbro (d) and monzonite porphyry (e) at Xiaokelehe.

CaO, Na_2O, K_2O and P_2O_5 contents and the SiO_2 contents (Fig. 7). These rocks are characterized by relatively enriched LREEs [$(La/Yb)_N$ = 13.56–13.78] and LILEs, but depleted HFSEs (incl. HREEs) and no Eu anomaly (δEu = 0.93–1.02) (Fig. 8a-b).

5.2.3. Monzonite

The rocks contain SiO_2 = 55.30–55.67 wt% (avg. 55.44 wt%), Total Fe_2O_3 = 6.44–6.68 wt% (avg. 6.54 wt%), and $Mg^{\#}$ = 40–41 (avg. 41). The samples are high-K calc-alkaline or shoshonite (Fig. 6b-c), and their A/CNK values (0.87–0.89) suggest that they are metaluminous (Fig. 6d). Meanwhile, their TFe_2O_3, MgO, TiO_2 and P_2O_5 contents show negative correlations with the SiO_2 contents (Fig. 7). The monzonite samples are enriched in LREEs [$(La/Yb)_N$ = 11.03–11.60], LILEs (Rb, Ba, K and Pb) and Sr (1160–1450 ppm), but depleted in HFSEs (HREEs, Nb, Ta and Ti), Cr (4.0–7.0 ppm), Ni (2.5–3.2 ppm) and Y contents (18.2–19.7 ppm), with lower Sr/Y ratios (63.6–73.6) and no obvious Eu anomaly (δEu = 0.89–0.92) (Fig. 8a-b).

5.2.4. Gabbro

The rocks have SiO_2 = 51.73–52.13 wt% (avg. 51.96 wt%), Total Fe_2O_3 = 8.48–8.71 wt% (avg. 8.63 wt%), and $Mg^{\#}$ = 50–51 (avg. 51). The gabbros are high-K calc-alkaline (Figs. 6b-c) and metaluminous (A/CNK = 0.85–0.91) (Fig. 6d). There are no clear correlations between the TiO_2, Al_2O_3, MgO, TFe_2O_3, CaO, Na_2O, K_2O and the SiO_2 contents (Fig. 7). The gabbros are featured by enrichments in LREEs [$(La/Yb)_N$ = 9.13–10.31], LILEs (Rb, Ba, K and Pb) and Sr contents (1270–1330 ppm), but depletions in HFSEs (HREEs, Nb, Ta and Ti), Cr (16.0–18.0 ppm), Ni (8.8–10.3 ppm) and Y (16.5–17.6 ppm), and with no Eu anomaly (δEu = 0.93–1.01) (Fig. 8a-b).

5.2.5. Monzonite porphyry

The rocks have SiO_2 = 60.37–60.90 wt% (avg. 60.59 wt%), Total Fe_2O_3 = 5.20–5.42 wt% (avg. 5.35 wt%), and $Mg^{\#}$ = 39–41 (avg. 40). The monzonite porphyry samples are classified as high-K calc-alkaline or shoshonite and metaluminous (A/CNK = 0.92–0.98) (Fig. 6a-c).

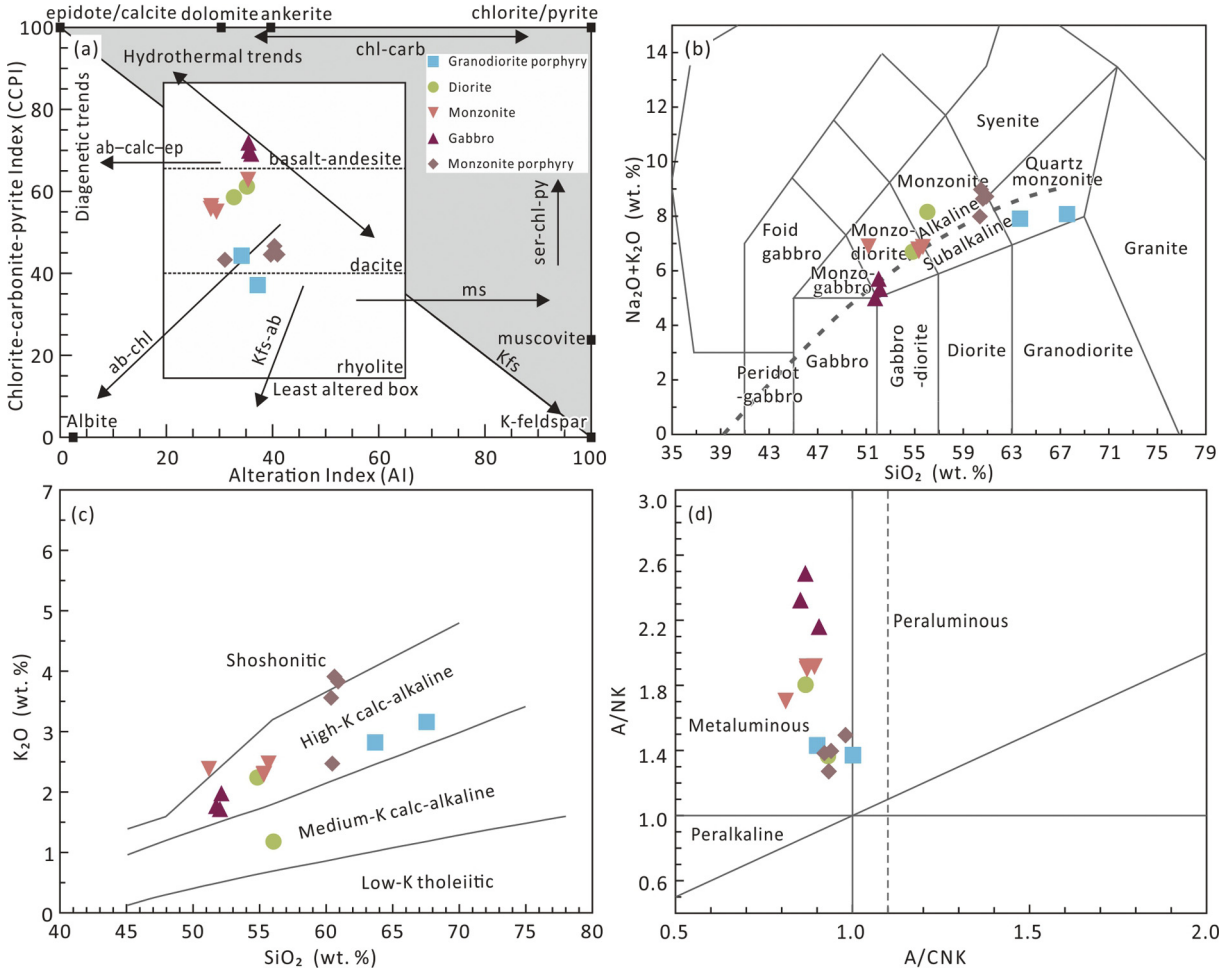

Fig. 6. Alteration box plot showing the major magmatic units in the Xiaokelehe Cu—Mo deposit (a, Large et al., 2001), plots of SiO_2 vs. ($Na_2O + K_2O$) (b, Baragar, 1971), SiO_2 vs. K_2O (c, Peccerillo and Taylor, 1976) and A/CNK vs. A/NK (d, Maniar and Piccoli, 1989) for the major magmatic units at Xiaokelehe.

There are no clear correlations between the TiO_2, Al_2O_3, MgO, TFe_2O_3, CaO, Na_2O, K_2O and the SiO_2 contents (Fig. 7). Additionally, these rocks are typically enriched in LREEs [$(La/Yb)_N = 11.19–14.58$], LILEs (Rb, Ba, K and Pb) and Sr contents (540–1035 ppm), but depleted in HFSEs (HREEs, Nb, Ta and Ti), Cr (3.0–4.0 ppm), Ni (0.9–1.3 ppm) and Y contents (22.7–24.1 ppm), with weak Eu negative anomaly ($\delta Eu = 0.77–0.83$) (Fig. 8a-b) and low Sr/Y ratios (21.5–43.9).

6. Discussion

6.1. Geochronological framework of Mesozoic magmatism in the GXR

As previous studies suggested, magmatism was widespread in the GXR from the Paleozoic to the Mesozoic, with abundant emplacement of granitoids (incl. granodiorite (porphyry), monzonite (porphyry), syenogranite, A-type rhyolite and alkaline granite) (Chen et al., 2017; Xu et al., 2013). These magmatic activities displayed a close space-time relationship with the regional Mesozoic porphyry-type mineralization, which was the most important porphyry-type mineralization episode in the GXR. Among the many porphyry-type deposits reported in the GXR, most were formed in the Mesozoic and minor formed in the Early Paleozoic (Chen et al., 2017). The Ordovician Duobaoshan and Tongshan porphyry Cu deposits (PCDs) (granodiorite = 479.5 ± 4.5 Ma; Chen et al., 2017) are the only few examples of the Paleozoic PCDs discovered in the GXR. In contrast, the many Mesozoic examples reported include the Wunugetushan PCD (180.5 ± 2.0 Ma; Wang et al., 2015), Taipingchuan PCD (202 ± 5.7 Ma, Chen et al., 2017), Chalukou porphyry Mo deposit (148 ± 1 Ma; Liu et al., 2013) and Fukeshan PCD (148.0 ± 2.8 Ma; Deng et al., 2019a). The ore-causative granitoids of these Mesozoic porphyry-type deposits were considered to be related to the subduction of the Mongol-Okhotsk oceanic plate (Deng et al., 2019a, 2019b; Wang et al., 2015) or post-collisional extension (Liu et al., 2013; Xu et al., 2013).

Compiling our zircon U—Pb ages with previous published data (Deng et al., 2019b), we suggested that Mesozoic magmatism at Xiaokelehe occurred intermittently at around 150 Ma, 146 Ma, 140 Ma and 123 Ma. The rhyolite (152.5 ± 1.7 Ma; Deng et al., 2019b) represents the earliest magmatic activity at Xiaokelehe and the main volcanic rock type in the area. For the ore-causative granodiorite, our zircon U—Pb data (148.9 ± 1.4 Ma) suggest that its emplacement was coeval with the mineralization within analytical uncertainties (molybdenite *Re*—Os age: 148.5 ± 1.5 Ma; Feng et al., 2020). Although the diorite (149.4 ± 4.0 Ma) and diorite porphyry (147.9 ± 1.3 Ma; Deng et al., 2019b) ages are similar to that of the granodiorite porphyry (within error), crosscutting relationships in drill cores suggest that the diorite (porphyry) was emplaced after the granodiorite porphyry (Fig. 3b-c). This is also true for the monzonite (146.9 ± 4.1 Ma), which is found intruding into the granodiorite porphyry (Fig. 3d). The gabbro (140.6 ± 3.8 Ma) and monzonite porphyry (139.9 ± 4.3 Ma) constitute the next magmatic phase, which agrees with the crosscutting relations that they intruded all the granodiorite porphyry, diorite and monzonite (Fig. 3e-f). Different from the granodiorite porphyry, diorite (porphyry) and monzonite, the gabbro and monzonite porphyry

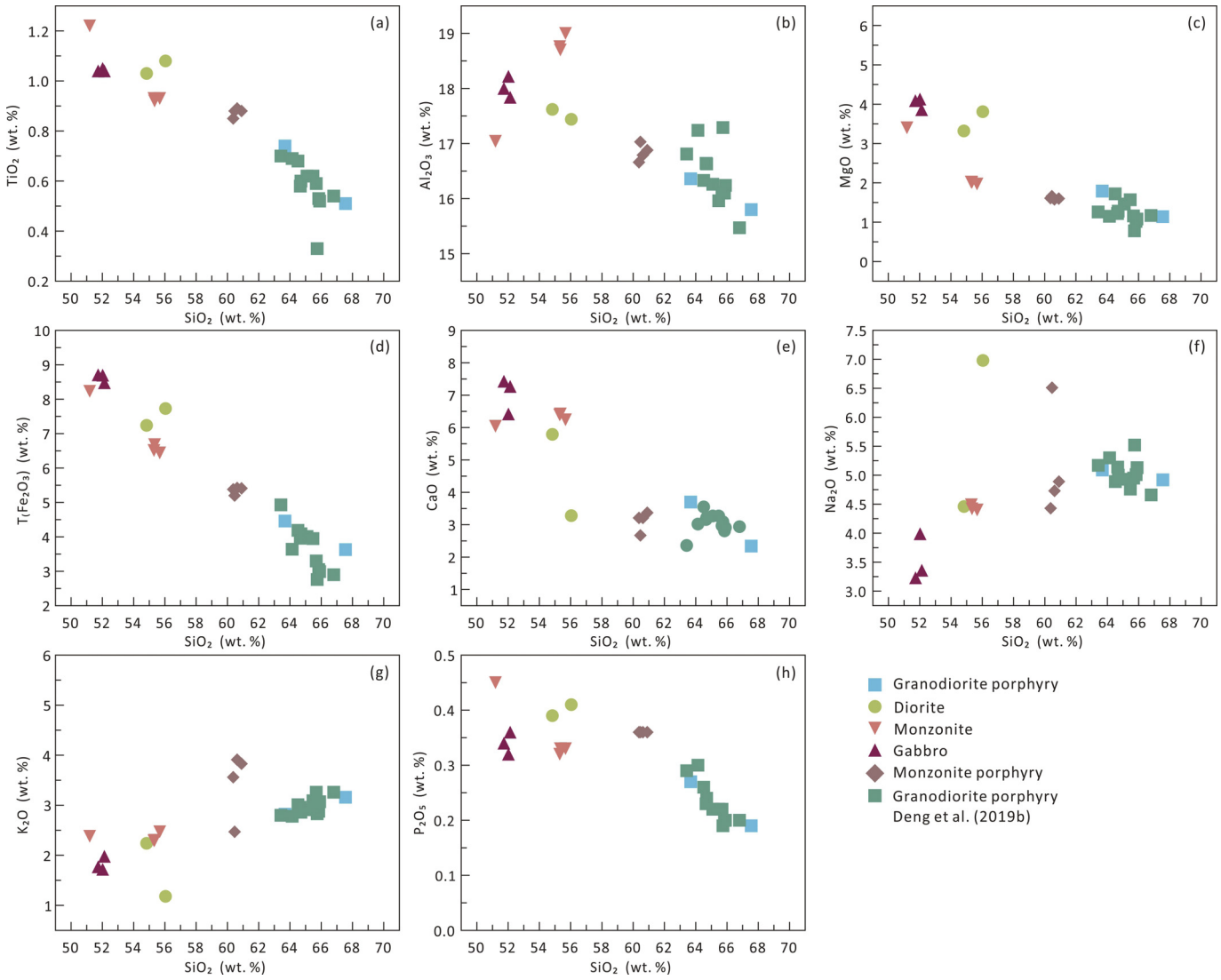

Fig. 7. Harker diagrams of the major magmatic units at Xiaokelehe.

have Precambrian inherited zircons, which were likely derived from the Xinghuadukou Group (Shang, 2017). The Xinghuadukou Group is considered to be the basement of the GXR. It is locally distributed in the Erguna and Xing'an terranes, and consists of schist and meta-plutonic rocks (Deng et al., 2019b). These inherited zircons suggest significant involvement of the Xinghuadukou Group in the magma evolution.

The ~123 Ma granite porphyry represents the latest magmatic activity at Xiaokelehe (123.2 ± 1.7 Ma; Deng et al., 2019b), as also demonstrated by that it intruded all other rock types in the area (Fig. 3i). Previous studies have identified four Mesozoic magmatic phases in the northern GXR: ca. 186–182 Ma (peak 183 Ma), 166–156 Ma (peak 163 Ma), 145–138 Ma (peak 143 Ma) and 128–106 Ma (peak 125 Ma) (Xu et al., 2013). At Xiaokelehe, the ~146 Ma and ~ 140 Ma magmatic activities fall inside the regional 145–138 Ma phase, whilst the ~128 Ma magmatic activities fall inside the regional 128–106 Ma phase (Fig. 9). The ~150 Ma magmatic activities at Xiaokelehe lie outside the four GXR magmatic phases. Yet magmatic rocks in the "156–145 Ma magmatic gap" were also reported at the Fukeshan PCD (148.7 ± 0.8 Ma; Deng et al., 2019a) and Chalukou Mo—Cu deposit (147.0 ± 0.8 Ma; Liu et al., 2013), probably indicating an unidentified new magmatic-metallogenic epoch in the GXR.

6.2. Petrogenesis of Late Mesozoic magmatism at Xiaokelehe

6.2.1. Granodiorite porphyry

As mentioned above, the granodiorite porphyry has adakite-like geochemical signatures. The term "adakite" was first proposed by Defant and Drummond (1990) to describe an unusual type of andesite that originated from partial melting of subducted oceanic plate. However, subsequent studies have shown that many igneous rocks with adakite-like geochemical features can be produced by other processes, including (1) partial melting of a peridotitic mantle that has been modified by slab melts (Martin et al., 2005), (2) delaminated mafic lower crust (Kay and Kay, 1993), (3) melting of thickened lower crust (Chung et al., 2003), (4) mixed origin (Li et al., 2013a; Zhou et al., 2015) and (5) fractional crystallization of mantle-derived magmas (Macpherson et al., 2006).

Previous studies have proposed that the Mongol-Okhotsk Ocean was closed in the Middle-Late Jurassic (Ren et al., 2016; Tang et al., 2016; Xu et al., 2013), which is also supported by our data (to be discussed below). Hence, the granodiorite porphyry was unlikely to be produced by partial melting of the subducting slab. Melts of the delaminated lower crust would likely interact and equilibrate with the mantle peridotite during they ascent, resulting in significantly elevated contents

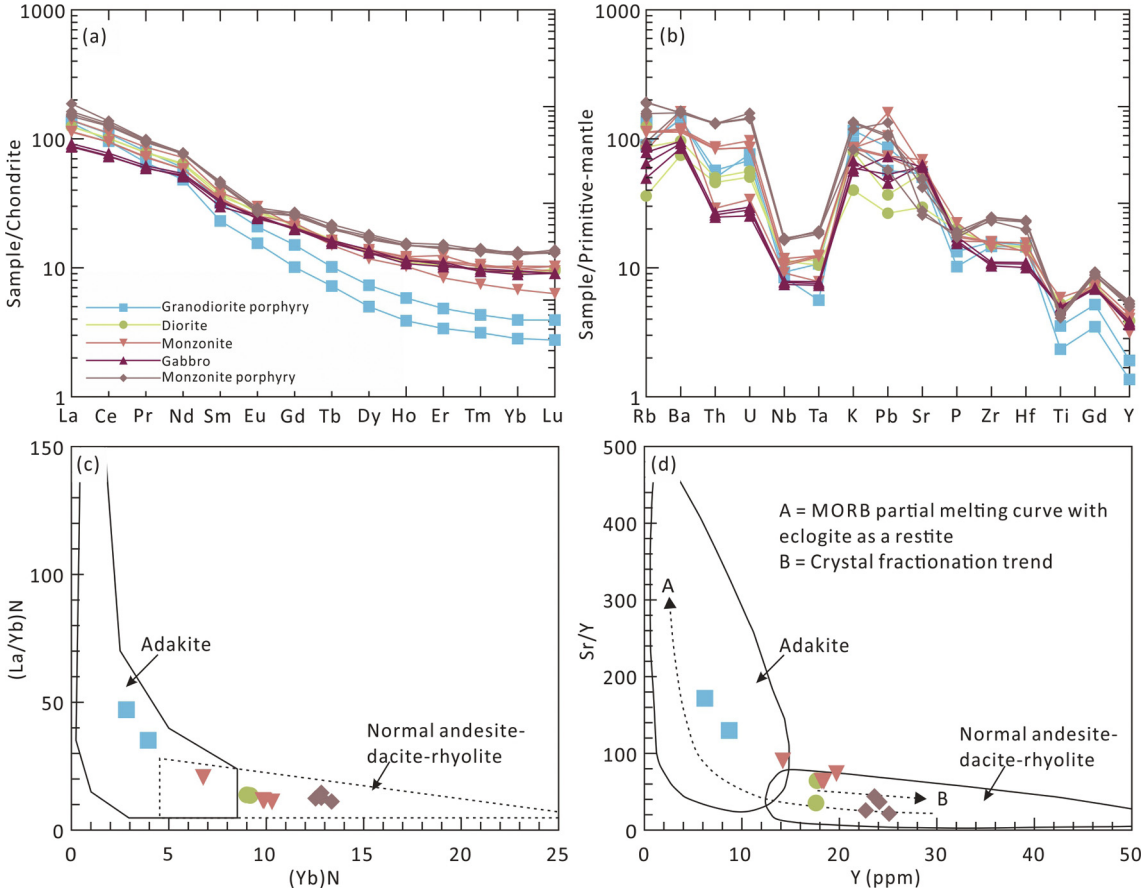

Fig. 8. Chondrite-normalized REE pattern (a, normalizing values from Sun and McDonough, 1989), primitive mantle-normalized trace elements web diagram (b, normalizing values from Sun and McDonough, 1989), plots of $(La/Yb)_N$ vs. Yb_N (c) and Sr/Y vs. Y (d) for the major magmatic units at Xiaokelehe.

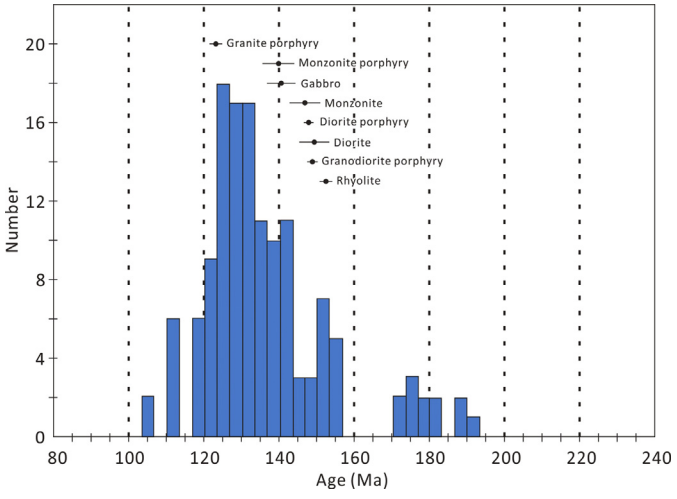

Fig. 9. Histogram of ages of Mesozoic igneous rocks in the GXR (Xu et al., 2013).

of MgO, Cr and Ni (Rapp et al., 1999). However, the lower Cr (29.0–31.0 ppm) and Ni (9.4–12.6 ppm) contents in the granodiorite porphyry are incompatible with this view. The granodiorite porphyry has higher MgO and $Mg^{\#}$ values than those of experimental melts by the partial melting of metabasalt and eclogite (Wang et al., 2006), inconsistent with the adakite derived from partial melting of the thickened lower crust (Rapp et al., 1999). As previous studies suggested, fractionation of mantle-derived basaltic melts could only form small volume of felsic magma (Zheng et al., 2015). Thus, large volume of basalts or gabbros is required to form the granodiorite porphyry at Xiaokelehe, which is not found in the outcrops or drill holes. At Xiaokelehe, mafic microgranular enclaves (MMEs) and zoned minerals (e.g., pyroxene, amphibole and plagioclase) are absent in the granodiorite porphyry. The granodiorite porphyry has relatively high $(^{87}Sr/^{86}Sr)_i$ ratios (0.7055–0.7057), low εNd(t) values (−1.2 to −0.3) and young T_{DM} model ages (0.83–0.90 Ga) (Deng et al., 2019b), indicating that they were derived from mantle-derived juvenile components without significant ancient crustal involvement. This is also supported by the lack of inherited zircons in the rocks (Fig. 5b). Therefore, a mixed magma source can be excluded.

Exclusions of the other possibilities lead to the conclusion that the Xiaokelehe granodiorite porphyry was formed by partial melting of the slab melt-modified peridotitic mantle. It is noted that the granodiorite porphyry samples have negative Nb—Ta anomalies (Fig. 8b), which are common in subduction-related (Sajona et al., 1993) or enriched subcontinental lithospheric mantle (SCLM)-derived (Whalen et al., 1996) magmas. Absence of arc magmatism at/around Xiaokelehe indicate that the observed Nb—Ta anomalies are most likely associated with an enriched SCLM source that reacted with subduction-related melts and/or fluids. The U—Th and Pb—Ce contents of the granodiorite porphyry (Figs. 10a-b) suggest that the mantle source was likely metasomatized by melts from the ancient-subducted slab and its sediments (Hawkesworth et al., 1997; Li et al., 2013b; Othman et al., 1989). The granodiorite porphyry has relatively high $(^{87}Sr/^{86}Sr)_i$ ratios (0.7055–0.7057) and low εNd(t) values (−1.2 to −0.3) (Deng et al., 2019b), indicating significant sediment input via crustal assimilation during the melt ascent or the above-mentioned metasomatism (Li et al., 2013b). As presented above, crustal contamination was likely unimportant for the granodiorite porphyry. Hence, we infer that the relatively

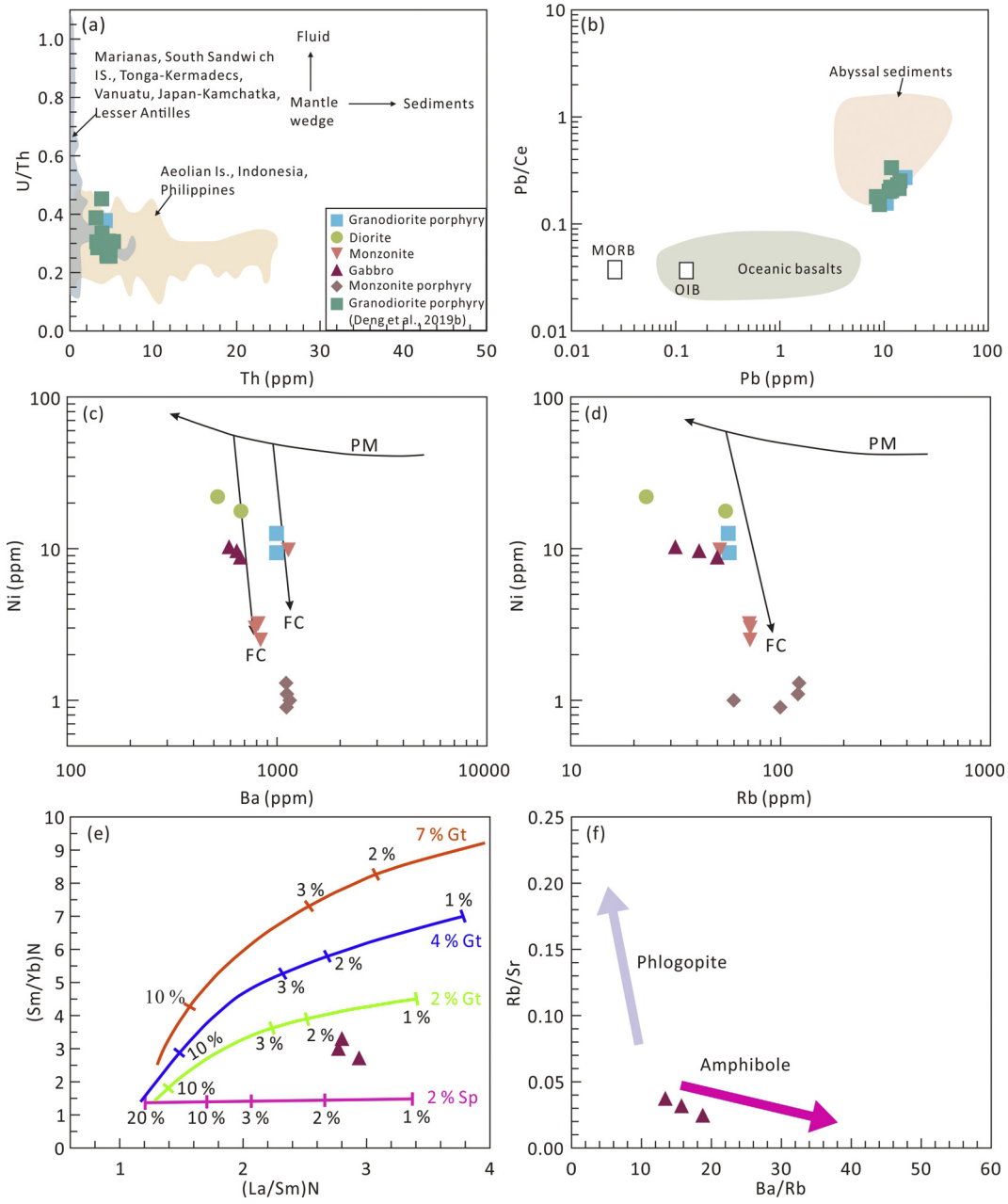

Fig. 10. Plots of (a) U/Th vs. Th (modified after Hawkesworth et al., 1997), (b) Pb/Ce vs. Pb (modified after Othman et al., 2006), (c) Ni vs. Ba, (d) Ni vs. Rb (modified after Wang et al., 2006), (e) $(La/Sm)_N$ vs. $(Sm/Yb)_N$ and (f) Ba/Rb vs. Rb/Sr for the Xiaokelehe magmatic rocks.

high Sr and low Nd isotope values of the granodiorite porphyry are generated in the magma source. This is supported by the contemporaneous, enriched mantle-derived basalts and andesites ($(^{87}Sr/^{86}Sr)_i$ = 0.705624–0.726886; εNd(t) = −1.83–0.69) in the northern GXR (Wu, 2006). Direct partial melts of an enriched mantle would be of basaltic composition with high $Mg^{\#}$ values (70–80, Li et al., 2009), and thus the granodiorite porphyry (with high SiO_2 (63.68–67.55 wt%) and low $Mg^{\#}$ (41–47)) cannot represent primary melts. Instead, the granodiorite porphyry was likely formed by fractionation (e.g., olivine) of the parental basaltic magma in depth. This model is consistent with those proposed for the granitoids at Tonglushan (Zhang et al., 2018), Daye (Li et al., 2009), Tongshankou, Chengmenshan, Wushan, Dongleiwan and Dengjiashan porphyries (Li et al., 2013b), and for the shoshonitic rocks at Luzong, Eastern China (Wang et al., 2006). Adakitic signatures (e.g., low HREE contents) were generally considered to be related to the presence of residual garnet in the magma source, as the garnet is the major host of HREEs (Defant and Drummond, 1990; Zheng et al., 2015).

In the Harker-type diagrams (Fig. 7), the negative correlations between SiO_2 and contents of TFe_2O_3, Al_2O_3, TiO_2, CaO, P_2O_5 and MgO indicate fractionation of hornblende, ilmenite, titanite and apatite. As expected, the relatively incompatible K increases with increasing SiO_2. There is no Na_2O vs. SiO_2 correlation or significant Sr and Eu anomalies, which indicate no major plagioclase fractionation or accumulation.

6.2.2. Diorite

The samples have chondrite-normalized REE and the primitive mantle-normalized trace element patterns similar to those of the granodiorite porphyry (Fig. 8a-b). This, and the close space-time relations between the diorite and granodiorite porphyry, suggest a possible genetic link. This implies that the dioritic magma was also evolved from the magma produced by partial melting of the lithospheric mantle

refertilized by slab-derived melts. Comparing to the granodiorite porphyry, the diorite is less HREE-depleted and less LREE/HREE fractionated, suggesting that the magma source has little residual garnet. Meanwhile, low Cr and Ni contents of the diorite indicate olivine fractionation at depth. The non-adakitic diorite has in general an order of magnitude higher Y contents and lower Sr contents than those of the adakite-like granodiorite porphyry (Fig. 8c-d), which was interpreted to be led by more plagioclase but less hornblende fractionation.

In the Ni vs. Ba and Ni vs. Rb diagrams (Fig. 10c-d), two diorite samples are plotted along the fractional crystallization trend, suggesting that fractionation had played an important role in the magmatic evolution. Two inherited zircons were found in the sample, possibly reflecting that crustal assimilation had occurred.

6.2.3. Monzonite and monzonite porphyry

The similarity in chondrite-normalized REE and the primitive mantle-normalized trace element patterns (Fig. 8a-b), together with the close spatial relations between the monzonite/monzonite porphyry and the granodiorite porphyry indicate possible genetic link between the former two. However, the low $Mg^{\#}$, Cr and Ni contents of the monzonite (porphyry) are not what would be expected if they were derived from the mantle (Martin et al., 2005). Hence, we infer that they were derived from partial melting of the lower crust. Comparing to the monzonite, the monzonite porphyry has lower Sr but higher HREE contents, together with negative Eu anomalies and weaker LREE/HREE fractionation (Fig. 8a-b). This suggests more plagioclase residue in the magma source for the monzonite porphyry compared to the monzonite. As previous studies suggested, plagioclase residue in the magma source suggest a magma formation depth of around 40 km (<1.2 GPa) (Rapp and Watson, 1995). Therefore, we consider that the monzonite was probably derived from partial melting of the thickened lower crust at >40 km, whist that for the monzonite porphyry was probably shallower (<40 km depth). Compared to typical adakitic rocks, both the monzonite and its porphyry have higher HREE and Y contents, but lower Sr and Sr/Y and weaker LREE/HREE fractionation, which indicate that no garnets were residual in the magma source.

In the Harker diagrams (Fig. 7), there are negative correlations between TFe_2O_3, TiO_2, P_2O_5 and MgO and SiO_2 contents of the monzonite (porphyry), suggesting the fractionation of pyroxene, ilmenite and apatite. The monzonite (porphyry) samples contain some inherited zircons, suggesting certain degree of crustal contamination. Meanwhile, the monzonite porphyry sample contains one Paleoproterozoic inherited zircon (2425 ± 23.6 Ma), which may be derived from the Xinhuadukou Group that is considered to be the basement of the GXR, and occasionally distributed in the Erguna and Xing'an terrane (Shang, 2017).

6.2.4. Gabbro

Partial melting experiment on anhydrous lherzolite also shows that the resulting partial melts would not be more felsic than andesites (~55 wt% SiO_2; Baker et al., 1995). Previous studies suggested that the gabbros derived from the asthenospheric mantle commonly have lower La/Nb (<1.5) and La/Ta (<22) ratios than those derived from the lithospheric mantle (Thompson and Morrison, 1988). The Xiaokelehe gabbros have high La/Nb (3.72–3.92) and La/Ta (66.12–69.33) ratios, indicating that they were derived from the lithospheric mantle. Moreover, the Xiaokelehe gabbros are characterized by LILE (incl. LREE) enrichments but HFSE (incl. HREE) depletions, resembling typical arc magmatic rocks (Zheng et al., 2015). This suggests that the lithospheric mantle source was metasomatized by arc-related fluids or sediments. The low Sr/Y and $(La/Yb)_N$ ratios, high HREEs and weak LREE/HREE fractionation of the Xiaokelehe gabbro imply that the mantle source did not contain residual garnet. Using the $(Sm/Yb)_N$ vs. $(La/Sm)_N$ diagram (Jourdan et al., 2007) and the equation of Shaw (1970) for non-modal melting, the Xiaokelehe gabbro can be modeled by 1–2% equilibrium melting of lherzolite with 2% spinel without garnet (Fig. 10e). Previous studies have suggested that the Nb/Ta ratio can distinguish high-pressure rutile-bearing phase from low-pressure amphibole-bearing phase. Amphibole-bearing phase is stable under <2.5 GPa, and would fractionate Nb/Ta ratios in the melts to low values (Foley et al., 2002). In contrast, the rutile-bearing phase is stable under >2.0 GPa and the Nb/Ta ratios are higher (Xiong et al., 2005). The Xiaokelehe gabbro has lower subchondritic Nb/Ta ratios (1.00–1.01), suggesting low-pressure amphibole residue in the mantle source. Meanwhile, the melts in equilibrium with amphibole have generally lower Rb/Sr and higher Ba/Rb ratios than those sourced from the phlogopite-bearing phase (Fig. 10f) (Furman and Graham, 1999). Therefore, the Xiaokelehe gabbro was likely derived from partial melting of amphibole-bearing lithospheric mantle metasomatized by slab melts. The low Cr and Ni contents of the rocks are in line with olivine-poor metasomatized lithospheric mantle.

In the Ni vs Ba and Ni vs Rb diagrams (Fig. 10c-d), the samples are plotted along the fractional crystallization trend, suggesting fractional crystallization plays an important role in the magma processes. Several Neoproterozoic and Paleoproterozoic inherited zircons were found in the gabbro, suggesting certain crustal assimilation during the magma ascent, as also supported by the high whole-rock Zr and Hf contents of the Xiaokelehe gabbro (Fig. 8b).

6.3. Geodynamic implications for the Late Mesozoic magmatism

As aforementioned, the Late Mesozoic GXR magmatism has been variably argued to be associated with the subduction of the Paleo-Pacific Ocean (Shu et al., 2016) or Mongol-Okhotsk Ocean (Deng et al., 2019a, 2019b; Donskaya et al., 2013), or post-collisional-related (Li et al., 2017a, 2017b; Sorokin et al., 2020; Xu et al., 2013). We favor the post-collision hypothesis because: (1) Mesozoic GXR magmatism likely occurred far (>2000 km) from the Paleo-Pacific subduction front; (2) Mesozoic magmatic rocks from the Lesser Xing'an-Zhangguangcai Range (between the GXR and Jihei region) constitute a typical bimodal assemblage (A-type granites and mafic-ultramafic rocks), suggestive of an extension tectonic regime (Xu et al., 2013); (3) seismological studies suggest that the back-arc extension led by the Paleo-Pacific subduction did not reach the Mesozoic GXR (Li et al., 2017a; Zheng et al., 2015).

Palaeomagnetic studies reveal that the Mongol-Okhotsk Ocean did not close in a scissor-like way until the end Early Cretaceous (Kravchinsky et al., 2002; Metelkin et al., 2010). Consequently, the northern GXR magmatism before that was more likely to be associated with the Mongol-Okhotsk Ocean subduction (Deng et al., 2019a, 2019b; Zhang, 2014). Deng et al. (2019b) found that the Late Jurassic granodiorite porphyry (150.0 Ma) at Xiaokelehe have arc-type adakitic affinities, and suggested that these rocks were formed by the south-dipping subduction of the Mongol-Okhotsk Ocean. However, there is no voluminous Late Jurassic basaltic-andesitic magmatism reported at/around Xiaokelehe. Slab-derived adakites are generally characterized by primitively low $(^{87}Sr/^{86}Sr)_i$ and high εNd(t) values (Defant and Drummond, 1990; Li et al., 2009), different from the Xiaokelehe granodiorite porphyry ($(^{87}Sr/^{86}Sr)_i$ = 0.7055–0.7057, εNd(t) = −1.2 to −0.3; Deng et al., 2019b), which indicates an enriched mantle source. Oceanic ridge subduction model on GXR proposed by Zhang (2014) is mainly based on the presence of widespread adakitic rocks, alkalic basalts and A-type granitoids. However, no alkali basalts were reported at Xiaokelehe. Meanwhile, all the Xiaokelehe porphyries (granodiorite, diorite and granite) have enriched Sr—Nd isotopic features ($(^{87}Sr/^{86}Sr)_i$ = 0.7054–0.7066; εNd(t) = −1.2–0.01; Deng et al., 2019b), inconsistent with a subducted oceanic ridge origin (Defant and Drummond, 1990; Li et al., 2009) and precluding the Mongol-Okhotsk oceanic ridge subduction model.

In addition, representativeness of published GXR palaeomagnetic data has been disputed, as most data from south of the Mongol-Okhotsk suture are from the North China plate (Ren et al., 2016). Thus, closure of the Mongol-Okhotsk Ocean until the end Early Cretaceous is questionable, which is also hard to reconcile with a number of

geological and geochemical facts. Geochemical and petrographic studies of the Middle-Upper Jurassic sandstone from the Mohe Basin (south of the Mongol-Okhotsk suture) suggested that the sediments were derived from the Mongol-Okhotsk suture zone, and indicated that the Mongol-Okhotsk Ocean was closed before the Middle Jurassic (Zhang, 2014). Sorokin et al. (2020) proposed that the Mongol-Okhotsk Ocean was finally closed in the Middle Jurassic (171 Ma), based on detrital zircon U-Pb-Hf isotopic data and whole-rock geochemical data of the metasedimentary rocks from north of the Mongol-Okhotsk suture. Sedimentary basin analyses east of the Mongol-Okhotsk suture also suggest that the Mongol-Okhotsk Ocean was finally closed in the Late Jurassic (Yang et al., 2015). In this study, the Late Mesozoic Xiaokelehe magmatic assemblage, including A-type rhyolite, and high-K calc-alkaline (granodiorite porphyry, diorite and gabbro) and shoshonitic (monzonite and its porphyry) intrusive rock, is also consistent with a post-collision extensional setting. Taken together, we support a pre-Late Jurassic closure of the Mongol-Okhotsk Ocean.

In a post-collision setting, a deep-sourced fluid-fluxed melting model was also proposed to explain the large-scale Early Cretaceous magmatism in the southern GXR. The model involves partial melting of the lithospheric mantle with fluid input (from ancient hydrated slab), which produced water-rich mafic magmas. These mafic magmas then underplated the lower crust and promoted water-fluxed partial melting there to form the large-scale Early Cretaceous magmatism (Li et al., 2017a, 2017b). However, magmatic rocks in the northern GXR are located far from the Mongol-Okhotsk suture and are likely unaffected by subduction or closure of the Mongol-Okhotsk Ocean. Thus, this model is unlikely to be applicable for the Xiaokelehe igneous rocks.

In brief, we suggest that after the collision between the Mongol-SinoKorea and Siberia plates (Fig. 11a), an extensional environment may have caused delamination of the thickened crust and asthenosphere upwelling (Wu, 2006; Xu et al., 2013). The melt (produced by partial melting of enriched mantle with garnet) may have fractionated during its ascent and formed the granodiorite porphyry (Fig. 11b). After the formation of the granodiorite porphyry, the enriched mantle (without garnet) metasomatized by subducted-related melts may have also partially melted. This melt was then also fractionated and experienced crustal contamination (mixing and homogenization) during their ascent, and formed the diorite that intruded into the granodiorite porphyry (Fig. 11b). During ca. 146–140 Ma, asthenospheric upwelling and partial melting of the lower crust persisted. Partial melting of the lower crust (without plagioclase) at depth > 40 km may have first occurred at ca. 146 Ma, corresponding to formation of the monzonite. Partial melting of the lower crust (with plagioclase) at depth < 40 km likely occurred at ca. 140 Ma, as marked by the emplacement of the monzonite porphyry, which has lower Sr, higher HREE contents, negative Eu anomalies, and weaker LREE/HREE fractionation than the monzonite (Fig. 11c). Intrusion of the Xiaokelehe gabbro happened at the same time, and its magma was likely derived from partial melting of a deep enriched-mantle (without garnet) source metasomatized by subduction-related melts (Fig. 11c).

At Xiaokelehe, pervasive alteration and Cu—Mo mineralization occurred in the granodiorite porphyry (Feng et al., 2019). As previous studies suggested, chalcophile elements in the mantle are mainly hosted in sulfides (Mungall, 2002). Removal of chalcophile elements

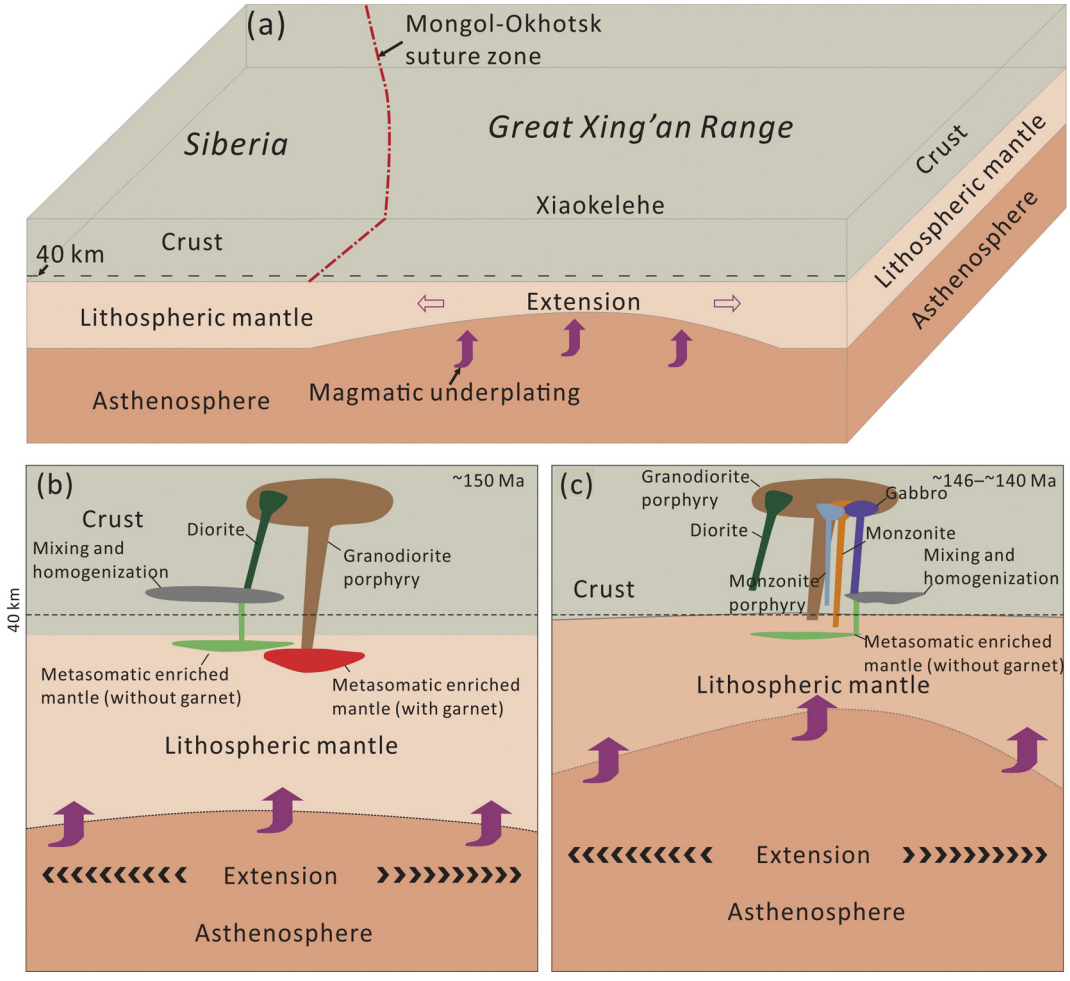

Fig. 11. Schematic geodynamic diagram showing the emplacement of the major Xiaokelehe magmatic units.

from the mantle by magmas required oxidizing conditions (log f_{O2} > FMQ (fayalite-magnetite-quartz oxygen buffer) + 2). The subducted oceanic upper crust has very high intrinsic f_{O2} due to equilibration with seawater during hydrothermal alteration and terrigenous sediment deposition (Mungall, 2002). Magmas derived from the enriched mantle (metasomatized by subduction-related melt) may have inherited the oxidizing character, melted/dissolved the mantle sulfides and scavenged their chalcophile metals. As a result, the granodiorite porphyry derived from an enriched mantle is favorable for porphyry Cu—Mo mineralization at Xiaokelehe. We infer, therefore, that the Late Mesozoic GXR was favorable for forming porphyry-type ore-causative intrusions in a post-collision setting after the Mongol-Okhotsk Ocean closure. This inference is supported by the many porphyry-type deposits newly-discovered in the GXR, including the Chalukou porphyry Mo deposit (147.0 ± 0.8 Ma; Liu et al., 2013), Fukeshan porphyry Cu—Mo deposit (148.0 ± 2.8 Ma; Deng et al., 2019a) and the Huluotai porphyry Cu—Mo deposit (150 ± 1 Ma; Deng et al., 2019c). The Chalukou Mo deposit (~30 km northwest of Xiaokelehe) has similar ore-formation ages (molybdenite *Re*—Os age: 147.0 ± 0.8 Ma; Liu et al., 2013) with Xiaokelehe (molybdenite Re—Os age: 148.5 ± 1.5 Ma; Feng et al., 2020), indicating a close space-time relation between the two. The coexistence of porphyry Cu (-Mo-Au) and porphyry Mo deposits are rarely reported, as porphyry Mo mineralization is commonly related to non-arc-related setting, e.g., the Dabie-East Qinling porphyry Mo belt in central China, where the Late Mesozoic porphyry Mo deposits were formed in post-collisional extension setting after the Paleo-Tethys closure (Li et al., 2007). Coexistence of these two porphyry-type mineralization is consistent with the post-collision setting in the Late Mesozoic GXR.

7. Conclusions

(1) LA-ICP-MS zircon U—Pb dating reveal that the magmatism at Xiaokelehe (granodiorite porphyry: 148.9 ± 1.4 Ma; diorite: 149.4 ± 4.0 Ma; monzonite: 146.9 ± 4.1 Ma; gabbro: 140.6 ± 3.8 Ma, and monzonite porphyry: 139.9 ± 4.3 Ma) was multiphase and occurred from the Late Jurassic to Early Cretaceous.

(2) The *syn*-ore granodiorite porphyry displays adakite-like affinity, and was derived from partial melting of the mantle (garnet-bearing) metasomatized by melts of previous-subducted slab and sediments in the upper part of oceanic crust. The post-ore diorite and gabbro were also derived from partial melting of the mantle (without garnet) metasomatized by melts of previous-subducted slab and sediments in the upper part of oceanic crust, and the post-ore monzonite (porphyry) magmas were sourced from the lower crust.

(3) The compressive to extensional transition after the collision between the Mongol-SinoKorea and Siberia plates may have caused the Late Mesozoic magmatism and porphyry Cu—Mo mineralization at Xiaokelehe.

Declaration of Competing Interest

The authors declare that they have no known competing financial interests or personal relationships that could have appeared to influence the work reported in this paper.

Acknowledgements

This research was financially supported by the National Natural Science Foundation of China (U1603244). Staffs of the Qiqihaer Mineral Exploration & Development Institute (Heilongjiang BGMR) are thanked for their support in granting access to drill cores and sample collection. We are grateful to Drs. Gaobin Chu and Lin Gong (GIGCAS) for their insightful suggestions on the paper.

Appendix A. Supplementary data

Supplementary data to this article can be found online at https://doi.org/10.1016/j.lithos.2020.105713.

References

Asadi, S., Moore, F., Zarasvandi, A., 2014. Discriminating productive and barren porphyry copper deposits in the southeastern part of the central Iranian volcano-plutonic belt, Kerman region, Iran: a review. Earth Sci. Rev. 138, 25–46.

Baker, M.B., Hischmann, M.M., Ghiorso, M.S., Stolper, E.M., 1995. Compositions of near-solidus predictive melts from experiments and thermodynamic calculations. Nature. 375, 308–311.

Cai, W., Wang, K., Li, J., Fu, L., Lai, C., Liu, H., 2020. Geology, geochronology and geochemistry of large Duobaoshan Cu-Mo-Au orefield in NE China: magma genesis and regional tectonic implications. Geosci. Front. https://doi.org/10.1016/j.gsf.2020.04.013 (in press).

Chen, Y.J., Zhang, C., Wang, P., Pirajno, F., Li, N., 2017. The Mo deposits of Northeast China: a powerful indicator of tectonic settings and associated evolutionary trends. Ore Geol. Rev. 81, 602–640.

Chung, S.L., Liu, D.Y., Ji, J.Q., Chu, M.F., Lee, H.Y., Wen, D.J., Zhang, Q., 2003. Adakites from continental collision zones: melting of thickened lower crust beneath southern Tibet. Geology. 31, 1021–1024.

Dai, M., Yan, G.S., Liu, C., Deng, J.F., Li, Y.S., Jia, W.B., Lai, C.K., 2020. Southward subduction of the Mongolia–Okhotsk Ocean: insights from early–middle Triassic intrusive rocks from the Jiawula–Tsagenbulagen area in NE China. Geol. J. 55, 967–993.

Defant, M.J., Drummond, M.S., 1990. Derivation of some modern arc magmas by melting of young subducted lithosphere. Nature. 347, 662–665.

Deng, C.Z., Li, G.H., 2019. The Cu-Mo mineralization of the late Jurassic porphyry in the Northern Great Xing'an Range: constraints from zircon U-Pb ages of the Ore-Causative Granites. Acta Geol. Sin. English Edn 93 (1), 236–237.

Deng, C.Z., Sun, D.Y., Ping, X.Q., Huang, H., Zhang, L.D., Lu, S., 2018a. Geochemistry of Early Cretaceous volcanic rocks in the Northeastern Great Xing'an Range, Northeast China and implication for geodynamic setting. Int. Geol. Rev. https://doi.org/10.1080/00206814.2018.1528481.

Deng, C.Z., Sun, G.Y., Sun, D.Y., Huang, H., Zhang, J.F., Gou, J., 2018b. Origin of C type adakite magmas in the NE Xing'an block, NE China and tectonic implication. Ac. Geochim. 37, 281–294.

Deng, C.Z., Sun, D.Y., Han, J.S., Chen, H.Y., Li, G.H., Xiao, B., Li, R.C., Feng, Y.Z., Li, C.L., Lu, S., 2019a. Late-stage southwards subduction of the Mongol-Okhotsk Ocean slab and implications for porphyry Cu-Mo mineralization: Constraints from igneous rocks associated with the Fukeshan deposit, NE China. Lithos. 326–327, 341–357.

Deng, C.Z., Sun, D.Y., Han, J.S., Li, G.H., Feng, Y.Z., Xiao, B., Li, R.C., Shi, H.L., Xu, G.Z., Yang, D.G., 2019b. Ages and petrogenesis of the late Mesozoic igneous rocks associated with the Xiaokele porphyry Cu-Mo deposit, NE China and their geodynamic implications. Ore Geol. Rev. 107, 417–433.

Donskaya, T.V., Gladkochub, D.P., Mazukabzov, A.M., Ivanov, A.V., 2013. Late Paleozoic-Mesozoic subduction related magmatism at the southern margin of the Siberian continent and the 150-million-year history of the Mongolia-Okhotsk ocean. J. Asian Earth Sci. 62, 79–97.

Feng, Y.Z., Xiao, B., Li, R.C., Deng, C.Z., Han, J.S., Wu, C., Li, G.H., Shi, H.L., Lai, C., 2019. Alteration mapping with short wavelength infrared (SWIR) spectroscopy on Xiaokelehe porphyry Cu-Mo deposit in the Great Xing'an Range, NE China: metallogenic and exploration implications. Ore Geol. Rev. 112, 103062.

Feng, Y.Z., Deng, C.Z., Chen, H.Y., Li, G.H., Xiao, B., Li, R.C., Shi, H.L., 2020. Re-Os isotopic dating of sulfides from the Xiaokelehe Cu-Mo deposit in the Northern part of the Great Xing'an Range, NE China, and its geological implications. Geotecton. Metallog. 3, 465–475.

Foley, S., Tiepolo, M., Vannucci, R., 2002. Growth of early continental crust controlled by melting of amphibolite in subduction zones. Nature. 417, 837–840.

Furman, T., Graham, D., 1999. Erosion of lithospheric mantle beneath the East African Rift system: geochemical evidence from the Kivu volcanic province. Lithos. 48, 237–262.

Hawkesworth, C.J., Turner, S.P., McDermott, F., Peate, D.W., van Calsteren, P., 1997. U-Th isotopes in arc magmas: implications for element transfer from subducted crust. Science. 276, 551–555.

Hoskin, P.W.O., Schaltegger, U., 2003. The composition of zircon and igneous and metamorphic petrogenesis. Rev. Mineral. Geochem. 53, 27–62.

Irvine, T.H., Baragar, W.R.A., 1971. A guide to the chemical classification of the common volcanic rocks. Can. J. Earth Sci. 8, 523–548.

Jourdan, F., Bertrand, H., Schaerer, U., Blichert-Toft, J., Feraud, G., Kampunzu, A.B., 2007. Major and trace element and Sr, Nd, Hf and Pb isotope compositions of the Karoo large igneous province, Botswana–Zimbabwe: lithosphere vs mantle plume contribution. J. Petrol. 48, 1043–1077.

Kay, R.W., Kay, S.M., 1993. Delamination and delamination magmatism. Tectonophysics. 219, 177–189.

Kravchinsky, V.A., Cogné, J.P., Harbert, W.P., Kuzmin, M.I., 2002. Evolution of the Mongol-Okhotsk Ocean as constrained by new palaeomagnetic data from the Mongol-Okhotsk suture zone, Siberia. Geophys. J. Int. 148 (1), 34–57.

Large, R.R., Gemmell, J.B., Paulick, H., Huston, D.L., 2001. The alteration box plot: a simple approach to understanding the relationships between alteration mineralogy and

lithogeochemistry associated with volcanic hosted massive sulfide deposits. Econ. Geol. 96, 957–971.
Li, N., Chen, Y.J., Zhang, H., Zhao, T.P., Deng, X.H., Wang, Y., Ni, Z.Y., 2007. Molybdenum deposits in East Qinling. Earth Sci. Front. 14 (5), 186–198.
Li, J.W., Zhao, X.F., Zhou, M.F., Ma, C.Q., Souza, Z.S., Vasconcelos, P., 2009. Late Mesozoic magmatism from the Daye region, eastern China: U-Pb ages, petrogenesis, and geodynamic implications. Contrib. Mineral. Petrol. 157, 383–409.
Li, S., Wang, T., Wilde, S.A., Tong, Y., 2013a. Evolution, source and tectonic significance of Early Mesozoic granitoid magmatism in the Central Asian Orogenic Belt (central segment). Earth Sci. Rev. 126, 206–234.
Li, X.H., Li, Z.X., Li, W.X., Wang, X.C., Gao, Y., 2013b. Revisiting the "C-type adakites" of the lower Yangtze River Belt, central eastern China: in-situ zircon Hf–O isotope and geochemical constraints. Chem. Geol. 345, 1–15.
Li, S., Chung, S.L., Wang, T., Wilde, S.A., Chu, M.F., Guo, Q.Q., 2017a. Tectonic significance and geodynamic processes of large-scale Early Cretaceous granitoid magmatic events in the southern Great Xing'an Range, North China. Tectonics. 36, 615–633.
Li, S., Chung, S.L., Wang, T., Wilde, S.A., Chu, M.F., Pang, C.J., Guo, Q.Q., 2017b. Water-fluxed crustal melting and petrogenesis of large-scale early cretaceous intracontinental granitoids in the southern Great Xing'an Range, North China. Geol. Soc. Am. 130 (3–4), 580–597.
Li, D.F., Tan, C.Y., Miao, F.Y., Liu, Q.F., Zhang, Y., Sun, X.M., 2019. Initiation of Zn-Pb mineralization in the Pingbao Pb-Zn skarn district, South China: constraints from U-Pb dating of grossular-rich garnet. Ore Geol. Rev. 107, 587–599.
Liu, Y.S., Hu, Z.C., Zong, K.Q., Gao, C., Gao, S., Xu, J., Chen, H., 2010. Reappraisement and refinement of zircon U–Pb isotope and trace element analyses by LA–ICP–MS. Chin. Sci. Bull. 55 (15), 1535–1546.
Liu, J., Wu, G., Wang, F., Luo, D.F., Hu, Y.Q., 2013. Geochronology and petrogeochemistry of Chalukou porphyry Mo deposit in northern Great Xing'an Range. Mineral Deposits 32 (6), 1093–1116.
Liu, H.C., Wang, J.C., Lai, C.K., Li, Y.L., Wang, J.F., Song, C.Y., Zhang, J.D., Zhao, X., Qin, J.D., 2020. Anatomy of two Permian greenschist- to blueschist-facies tectonic mélanges in the Solonker Suture Zone (Inner Mongolia, northeastern China): evidence for divergent double subduction and soft collision. J. Geol. Soc. Lond. https://doi.org/10.1144/jgs2020-006 (in press).
Ludwig, K.R., 2003. ISOPLOT 3.00: A Geochronological Toolkit for Microsoft Excel. Berkeley Geochronology Center, California, Berkeley, p. 39.
Macpherson, C.G., Dreher, S.T., Thirlwall, M.F., 2006. Adakites without slab melting: high pressure differentiation of island arc magma, Mindanao, the Philippines. Earth Planet. Sci. Lett. 243, 581–593.
Maniar, P.D., Piccoli, P.M., 1989. Tectonic discrimination of granitoids. Geol. Soc. Am. Bull. 101 (5), 635–643.
Martin, H., Smithies, R.H., Rapp, R., Moyen, J.F., Champion, D., 2005. An overview of adakite, tonalite–trondhjemite–granodiorite (TTG), and sanukitoid: relationships and some implications for crustal evolution. Lithos. 79, 1–24.
Metelkin, D.V., Vemikovsky, V.A., Kazansky, A.Y., Wingate, M.T., 2010. Late Mesozoic tectonics of Central Asia based on paleomagnetic evidence. Gondwana Res. 18 (2), 400–419.
Mungall, J.E., 2002. Roasting the mantle: slab melting and the genesis of major au and Au-rich Cu deposits. Geology. 30, 915–918.
Othman, D.B., White, W.M., Patchett, J., 1989. Geochemistry of marine sediments, island arc magma genesis and crust–mantle recycling. Earth Planet. Sci. Lett. 94, 1–21.
Peccerillo, A., Taylor, A.R., 1976. Geochemistry of Eocene calc-alkaline volcanic rocks from the Kastamonu area, Northern Turkey. Contrib. Mineral. Petrol. 58 (1), 63–81.
Rapp, R.P., Watson, E.B., 1995. Dehydration melting of metabasalt at 8–32 kbar: implications for continental growth and crustal recycling. J. Petrol. 36, 891–931.
Rapp, R.P., Shimizu, N., Norman, M.D., Applegate, G.S., 1999. Reaction between slab-derived melts and peridotite in the mantle wedge: experimental constraints at 3.8 GPa. Chem. Geol. 160, 335–356.
Ren, Q., Zhang, S., Wu, H., Liang, Z., Miao, X., Zhao, H., Li, H., Yang, T., Pei, J., Davis, G.A., 2016. Further paleomagnetic results from the ~155 Ma Tiaojishan Formation, Yanshan Belt, North China, and their implications for the tectonic evolution of the Mongol-Okhotsk suture. Gondwana Res. 35, 180–191.
Sajona, F.G., Maury, R.C., Bellon, H., Cotton, J., Defant, M.J., Pubellier, M., 1993. Initiation of subduction and the generation of slab melts in western and eastern Mindanao, Philippines. Geology. 21, 1007–1010.
Shang, Y.G., 2017. Geological Characteristics and Metallogenic Prognosis of Xiaokele and 972 Highland Gold Polymetallic Deposit in Daxinganling. Jilin University, Changchun, pp. 1–116 (in Chinese with English abstract).
Shaw, D.M., 1970. Trace element fractionation during anatexis. Geochim. Cosmochim. Acta 34, 237–243.
Shu, Q., Chang, Z., Lai, Y., Zhou, Y., Sun, Y., Yan, C., 2016. Regional metallogeny of Mo-bearing deposits in northeastern China, with new Re-Os dates of porphyry Mo deposits in the northern Xilamulun district. Econ. Geol. 111 (7), 1783–1798.
Sorokin, A.A., Zaika, V.A., Kovach, V.P., Kotov, A.B., Xu, W.L., Yang, H., 2020. Timing of closure of the eastern Mongol-Okhotsk Ocean: constrains from U-Pb and Hf isotopic data of detrital zircons from metasediments along the Dzhagdy Transect. Gondwana Res. 81, 58–78.
Tang, J., Xu, W.L., Wang, F., Zhao, S., Wang, W., 2016. Early Mesozoic southward subduction history of the Mongol–Okhotsk oceanic plate: evidence from geochronology and geochemistry of Early Mesozoic intrusive rocks in the Erguna Massif, NE China. Gondwana Res. 31, 218–240.
Thompson, R.N., Morrison, M.A., 1988. Asthenospheric and lower-lithospheric mantle contributions to continental extensional magmatism: an example from the British Tertiary Province. Chem. Geol. 68, 1–15.
Wang, Q., Wyman, D.A., Xu, J.F., Zhao, Z.H., Jian, P., Xiong, X.L., Bao, Z.W., Li, C.F., Bai, Z.H., 2006. Petrogenesis of cretaceous adakitic and shoshonitic igneous rocks in the Luzong area, Anhui Province (eastern China): implications for geodynamics and Cu-Au mineralization. Lithos. 89, 424–446.
Wang, Y., Zhao, C., Zhang, F., Liu, J., Wang, J., Peng, R., Liu, B., 2015. SIMS zircon U–Pb and molybdenite Re–Os geochronology, Hf isotope, and whole-rock geochemistry of the Wunugetushan porphyry Cu–Mo deposit and granitoids in NE China and their geological significance. Gondwana Res. 28 (3), 1228–1245.
Whalen, J.B., Jenner, G.A., Longstaffe, F.J., 1996. Geochemical and isotopic (O, Nd, Pb and Sr) constraints on A-type granite petrogenesis based on the Topsails Igneous Suite, Newfoundland Appalachians. J. Petrol. 87, 1463–1489.
Wu, G., 2006. Metallogenic Setting and Metallogenesis of Nonferrous-Precious Metals in Northern Da Hinggan Mountain. Jilin University, Changchun, pp. 21–30 (in Chinese with English abstract).
Xiong, X.L., Adam, J., Green, T.H., 2005. Rutile stability and rutile/melt HFSE partitioning during partial melting of hydrous basalt: implications for TTG genesis. Chem. Geol. 218, 339–359.
Xu, W.L., Pei, F.P., Wang, F., Meng, E., Ji, W.Q., Yang, D.B., Wang, W., 2013. Spatial–temporal relationships of Mesozoic volcanic rocks in NE China: constraints on tectonic overprinting and transformations between multiple tectonic regimes. J. Asian Earth Sci. 74, 167–193.
Yang, Y.T., Guo, Z.X., Song, C.C., Li, X.B., He, S., 2015. A short-lived but significant Mongol–Okhotsk collisional orogeny in latest Jurassic–earliest Cretaceous. Gondwana Res. 28 (3), 1096–1116.
Zhang, K.J., 2014. Genesis of the Late Mesozoic Great Xing'an range large igneous province: a Mongol-Okhotsk slab window model. Int. Geol. Rev. 13, 1557–1583.
Zhang, S.T., Chen, H.Y., Han, J.S., Zhang, Y., Chu, G.B., Wei, K.T., Zhao, Y.J., Cheng, J.M., Tian, J., 2018. Geochronology, geochemistry, and mineralization of quartz monzodiorite and quartz monzodiorite porphyry in Tonglushan Cu-Fe-Au deposit, Edongnan ore district, China. Geochimica. 47, 240–256.
Zhang, Y., Cheng, J.M., Tian, J., Pan, J., Sun, S.Q., Zhang, L.J., Zhang, S.T., Chu, G.B., Zhao, Y.J., Lai, C., 2019. Texture and trace element geochemistry of quartz in skarn system: perspective from Jiguanzui Cu-au skarn deposit, Eastern China. Ore Geol. Rev. 109, 535–544.
Zheng, Y.F., Chen, Y.X., Dai, L.Q., Zhao, Z.F., 2015. Developing plate tectonics theory from oceanic subduction zones to collisional orogens. Sci. China Earth Sci. 58, 1045–1069.
Zhou, T.F., Wang, S.W., Fan, Y., Yuan, F., Zhang, D.Y., White, N.C., 2015. A review of the intracontinental porphyry deposits in the Middle-lower Yangtze River Valley metallogenic belt, Eastern China. Ore Geol. Rev. 65, 433–456.